

Arctic sea ice-free season projected to extend into fall

Marion Lebrun¹, Martin Vancoppenolle¹, Gurvan Madec¹, François Massonnet^{2,3}

¹ Sorbonne Université, LOCEAN-IPSL, CNRS/IRD/MNHN, Paris, France

² Earth and Life Institute, Université catholique de Louvain, Louvain-la-Neuve, Belgium

³ Earth Sciences Department, Barcelona Supercomputing Center, Barcelona, Spain

Revised manuscript submitted to *The Cryosphere*

Dec 12, 2018

Marion Lebrun, Laboratoire d'Océanographie et du Climat, IPSL Boite 100, 4 Place Jussieu, 75252
Paris CEDEX 05, France.

22 **Abstract**

23 The recent Arctic sea-ice reduction comes with an increase in the ice-free season duration, with
24 comparable contributions of earlier ice retreat and later advance. CMIP5 models all project that the
25 trend towards later advance should progressively exceed and ultimately double the trend towards
26 earlier retreat, causing the ice-free season to shift into fall. We show that such shift is a basic feature
27 of the thermodynamic response of seasonal ice to warming. The detailed analysis of an idealised
28 thermodynamic ice-ocean model stresses the role of two seasonal amplifying feedbacks. The
29 summer feedback generates a 1.6-day later advance in response to a 1-day earlier retreat. The
30 underlying physics are the property of the upper ocean to absorb solar radiation more efficiently
31 than it can release heat right before ice advance. The winter feedback is comparatively weak,
32 prompting a 0.3-day earlier retreat in response to a 1-day shift towards later advance. This is
33 because a shorter growth season implies thinner ice, that subsequently melts away faster. However,
34 the winter feedback is dampened by the relatively long ice growth period and by the inverse
35 relationship between ice growth rate and thickness. At inter-annual time-scales, the thermodynamic
36 response of ice seasonality to warming is obscured by inter-annual variability. Nevertheless, on the
37 long term, because all feedback mechanisms relate to basic and stable elements of the Arctic
38 climate system, there is little inter-model uncertainty on the projected long-term shift into fall of the
39 ice-free season.

40

41

42 **1. Introduction**

43 Arctic sea ice has strikingly declined in coverage (Cavalieri and Parkinson, 2012), thickness
44 (Kwok and Rothrock, 2009; Renner et al., 2014; Lindsay and Schweiger, 2015) and age (Maslanik et
45 al., 2011) over the last four decades. CMIP5 global climate and Earth System Models simulate and
46 project this decline to continue over the 21st century (Massonnet et al., 2012; Stroeve et al., 2012) due
47 to anthropogenic CO₂ emissions (Notz and Stroeve, 2016), with a loss of multi-year ice estimated for
48 2040-2060 (Massonnet et al., 2012), in the case of a business-as-usual emission scenario.

49 Less Arctic sea ice also implies changes in ice seasonality, which are important to investigate
50 because of socio-economic (e.g., on shipping, Smith and Stephenson, 2013) and ecosystem
51 implications. Indeed, the length of the Arctic sea ice season exerts a first-order control on the light
52 reaching phytoplankton (Arrigo and van Dijken, 2011; Wassmann and Reigstad, 2011, Assmy et al.,
53 2017) and is crucial to some marine mammals, such as walruses (Laidre et al., 2015) and polar bears
54 (Stern and Laidre, 2016), who use sea ice as a living platform.

55 Various seasonality diagnostics are discussed in the sea ice literature and definitions as well as
56 approaches vary among authors. The open water season duration can be diagnosed from satellite ice
57 concentration fields, either as the number of ice-free days (Parkinson et al., 2014), or as the time
58 elapsed between ice retreat and advance dates, corresponding to the day of the year when ice
59 concentration exceeds or falls under a given threshold (Stammerjohn et al., 2012; Stroeve et al.,
60 2016). The different definitions of the length of the open water season can differ in subtleties of the
61 computations (notably filtering) and may not always entirely be consistent and comparable. In
62 addition, the melt season duration, distinct from the open water season duration, has also been
63 analysed from changes in passive microwave emission signals due to the transition from a dry to a
64 wet surface during melting (Markus et al., 2009; Stroeve et al., 2014).

65 As for changes in the Arctic open water season duration, satellite-based studies indicate an
66 increase by >5 days per decade over 1979-2013 (Parkinson, 2014) due to earlier ice retreat and later

67 advance (Stammerjohn et al., 2012; Stroeve et al., 2016). There are regional deviations in the
68 contributions to a longer open water season duration, most remarkably in the Chukchi and Beaufort
69 Seas where later ice advance takes over (Johnson and Eicken, 2016; Serreze et al., 2016), which has
70 been attributed to increased oceanic heat advection from Bering Strait (Serreze et al., 2016). Such
71 changes in the seasonality of Arctic ice-covered waters reflect the response of the surface energy
72 budget to warming. Indeed, warming and ice thinning imply earlier surface melt onset and ice retreat
73 (Markus et al., 2009; Stammerjohn et al., 2012; Blanchard-Wrigglesworth et al., 2010). Besides, a
74 shift towards later ice advance, tightly co-located with earlier retreat is observed, especially where
75 negative sea-ice trends are large (Stammerjohn et al., 2012; Stroeve et al., 2016). This has been
76 attributed to the ice-albedo feedback, namely to the combined action of (i) earlier ice retreat, implying
77 lower surface albedo and (ii) higher annual solar radiation uptake by the ocean. Such mechanism
78 (Stammerjohn et al., 2012) explains the ongoing delay in ice advance of a few days per decade from
79 the estimated increase in solar absorption (Perovich et al., 2007), in accord with the observed in situ
80 increase in the annual SST maximum (Steele et al., 2008; Steele and Dickinson, 2016).

81 The observed increase in the ice-free season duration should continue over the next century, as
82 projected by the CESM-Large Ensemble (Barnhart et al., 2016), but this signal is obscured by
83 important levels of internal variability. Other CMIP5 ESMs likely project a longer ice-free season as
84 well, and this is true in the Alaskan Arctic where they have been analysed (Wang and Overland,
85 2015). In both these studies, the simulated future increases in the ice-free season duration are
86 dominated by the later ice advance. Such behaviour remains unexplained and should be investigated
87 from a larger set of models and regions.

88 In the present study, we aim at better quantifying the potential changes in Arctic sea ice
89 seasonality and understanding the associated mechanisms. We first revisit the ongoing changes in
90 Arctic sea ice retreat and advance dates using satellite passive microwave records, both at inter-annual
91 and multi-decadal time scales. We also analyse, for the first time over the entire Arctic, all CMIP5

92 historical and RCP8.5 simulations covering 1900-2300 and study mechanisms at play using a one-
93 dimensional ice-ocean model.

94 **2. Methods**

95 We analyse the recent past and future of sea ice seasonality by computing a series of
96 diagnostics based on satellite observations, Earth System Models and a simple ice-ocean model.

97

98 **2.1 Data sources**

99 Passive microwave sea ice concentration (SIC) retrievals, namely the GSFC Bootstrap
100 SMMR-SSM/I quasi-daily time series product, over 1980-2015 (Comiso, 2000, updated 2015), are
101 used as an observational basis. We also use CMIP5 Earth System Model historical simulations and
102 future projections of SIC. Because of high inter-annual variability in ice advance and retreat dates
103 and because some models lose multi-year ice only late into the 21st century, we retain the 9 ESMs
104 simulations that pursue RCP8.5 until 2300 (first ensemble member, Table 1). Analysis focuses on
105 1900-2200, combining historical (1900-2005) and RCP8.5 (2005-2200) simulations. 2200
106 corresponds to the typical date of year-round Arctic sea ice disappearance (Hezel et al., 2014). We
107 also extracted the daily SST output from IPSL-CM5A-LR. All model outputs were interpolated on a
108 1° geographic grid.

109 To investigate how mean state biases may affect ESM simulations, we also included in our
110 analysis a 1958-2015 forced-atmosphere ISPL-CM simulation, i.e. an ice-ocean simulation that was
111 performed with the NEMO-LIM 3.6 model (Rousset et al., 2015), driven by the DFS5 atmospheric
112 forcing (Dussin et al., 2015). NEMO-LIM 3.6 is similar to the ice-ocean component of IPSL-
113 CM5A-LR, except that (i) horizontal resolution is twice as high (1° with refinement near the poles
114 and the equator) (ii) the sea ice model has been upgraded to multiple categories, among other
115 differences and (iii) a weak sea surface salinity restoring is applied. Such a simulation, not only
116 performs generally better than a free-atmosphere ESM run in terms of seasonal ice extent (Fig S1;
117 Uotila et al., 2017), but also has year-to-year variations in phase with observations, a feature that is
118 intrinsically not captured in a coupled ESM. However, a caveat of forced-atmosphere simulations is

119 the absence of feedback from the sea ice/ocean surface state onto atmospheric conditions, which
120 can affect the processes that drive changes in ice advance and retreat timing.

121 **2.2 Ice seasonality diagnostics**

122 We use slightly updated computation methods for ice retreat (d_r) and advance (d_a) dates, as
123 compared with previous contributions (Parkinson, 1994; Stammerjohn et al., 2012; and Stroeve et al.,
124 2016). Ice retreat date (d_r) is defined as the first day of the year where SIC drops below 15%, whereas
125 ice advance date (d_a) is the first day of the year where SIC exceeds this threshold (Stroeve et al, 2016).
126 The choice of the SIC threshold has no significant impact on the results. All previous studies
127 recognise that a typical 5-day temporal filtering on the input ice concentration is required to get rid
128 of short-term dynamical events (Stammerjohn et al., 2012; Stroeve et al., 2016). By contrast, we use
129 15 days, in order to get rid of most short-term dynamical ice events, which barely affects trends in d_r
130 and d_a (see Table S1). Another important issue is the reference time axis, which varies among authors.
131 To circumvent the effect of the d_a discontinuity between Dec 31 and Jan 1, we define the origin of
132 time on Jan 1, and count d_a negatively if it falls between Jul 1 and Dec 31. Jul 1 is a safe limit, because
133 there is no instance of ice advance date between early June and late July in the satellite record or in
134 CMIP5 simulations. The length of the ice-free season is defined as the period during which SIC is
135 lower than 15%.

136 The same seasonality diagnostics are computed from model outputs. Yet, since the long-term
137 ESM simulations used here only have monthly SIC outputs, we compute the ice seasonality
138 diagnostics based on monthly SIC fields linearly interpolated daily. Such operation drastically
139 reduces error dispersion but introduces a small systematic bias on d_r (early bias) and d_a (late bias), on
140 the order of 5 ± 5 (6) days. These biases were determined from an analogous processing of satellite
141 records. Dates of ice retreat and advance were derived from a daily interpolation of monthly averaged
142 concentration fields, and subsequently compared to direct retrievals based on daily resolved
143 concentration fields (see Fig S2). The identified biases apply to CMIP5 records, because errors stem
144 from the processing of data, and do not depend on the type of data used (satellite or CMIP5). These

145 small systematic biases in model ice retreat and advance dates likely contributes to the mean model
146 bias compared to satellite data (Table 1, Fig. 1), but remains small compared to the long-term signals
147 analysed throughout this paper.

148 The ice seasonality diagnostics and their spatial distribution are reasonably well captured by
149 the mean of selected CMIP5 models over the recent past (Fig. 2). The spatial distribution of ice
150 seasonality diagnostics varies among models, reflecting a possible dependence on the mean state or
151 differences in the treatment of ice dynamics. Larger errors in some individual models (Fig. S3) are
152 associated with an inaccurate position of the ice edge. Overall, ESMs tend to have a shorter open
153 water season than observed (Fig 2a-c and S3), which is visible in the North Atlantic and North Pacific
154 regions and can be related to the systematic bias due to the use of interpolated monthly data, but also
155 to the tendency of our model subset to overestimate sea ice. Such an interpretation is supported by (i)
156 the visibly better consistency of the simulated ice seasonality diagnostics with observations in the
157 forced-atmosphere ISPL-CM simulation than in IPSL-CM5A-LR and (ii) by the fact that models with
158 simulated ice extent rather close to observations over the recent past (CESM, CNRM or MPI;
159 Massonnet et al., 2013) are more in line with observed seasonality diagnostics than the other models
160 (Fig. 2 and S3).

161 **2.3. Trends in ice advance and retreat dates, and related diagnostics**

162 Trends in ice retreat and advance dates were calculated for each satellite or model pixel, from
163 the slope of a least-square fit over a given period, using years where both d_r and d_a are defined. If the
164 number of years used for calculation of the trend is less than 1/3 of the considered period, a missing
165 value is assigned. 1/3 compromises between spatial and temporal coverage of the considered time-
166 series (see Tab. S1).

167 To describe the relative contribution of ice advance and retreat dates to changes in open water
168 season duration, we introduce a first diagnostic, termed the *long-term ice advance vs. retreat*
169 *amplification coefficient* ($R_{a/r}^{long}$). $R_{a/r}^{long}$ is defined as minus the ratio of trends in ice advance to trends
170 in ice retreat dates. The sign choice for $R_{a/r}^{long}$ is such that positive values arise for concomitant long-

term trends toward later ice advance and earlier retreat. $R_{a/r}^{long}$ gives synthetic information about trends in ice advance and retreat dates within a single diagnostic. For example, $R_{a/r}^{long} > 0$ means that a trend towards earlier retreat ($d_r < 0$) occurs concurrently with a trend towards later advance ($d_a > 0$). Strictly speaking $R_{a/r}^{long} > 0$ could also indicate later retreat and earlier advance (i.e. a reduction of open water season duration), which does not happen in a warming climate. Moreover, by definition, $R_{a/r}^{long} > 1$ if the long-term trend in ice advance date exceeds the long-term trend in retreat date in a particular pixel, otherwise $R_{a/r}^{long} < 1$. Note that for $R_{a/r}^{long}$ to be meaningful, we restrict computations to pixels where trends in both d_r and d_a are significant at a specified confidence level. $p=0.05$, i.e a 95% confidence interval gives the most robust value but heavily restricts the spatial coverage, especially for CMIP5 outputs. By contrast, $p=0.25$, i.e. a 75% confidence interval slightly expands coverage, but loses some robustness.

In order to study the shorter-term association between retreat and ice advance, we introduce a second diagnostic, termed the *short-term ice advance vs retreat amplification coefficient* ($R_{a/r}^{short}$). $R_{a/r}^{short}$ is defined by applying the same reasoning to inter-annual time scales, as minus the linear regression coefficient between detrended ice advance and retreat dates. $R_{a/r}^{short}$ gives information on how anomalies in ice advance date scale with respect to anomalies in retreat dates over the same year, regardless of the long-term trend. Such definition warrants comparable interpretation for $R_{a/r}^{short}$ and $R_{a/r}^{long}$. In a warming climate, $R_{a/r}^{short} > 0$ indicates concomitant anomalies towards earlier retreat and later advance, and $R_{a/r}^{short} > 1$ indicates that anomalies in advance date are larger than in retreat date.

For computations of $R_{a/r}^{long}$ and $R_{a/r}^{short}$ we use a reference period of 36 years. 36 years is the length of the available observation period and is close to the standard 30 years used in climate sciences. In one occasion (Table 1), we use 200 years as a reference period. 200 years is the total amount of years we can use to qualify changes and the most representative of a long climate change simulation.

195 All trends and ice advance vs. retreat amplification coefficients given in the rest of the text are
196 median (\pm inter-quartile range), taken over the seasonal ice zone. We use non-parametric statistics
197 because the distributions are not Gaussian.

198

199 **2.4 1D model**

200 We use the Semtner (1976) zero-layer approach for ice growth and melt above an upper
201 oceanic layer taking up heat, whereas snow is neglected. The model simplifies reality by assuming
202 constant mixed-layer depth, no horizontal advection in ice and ocean, no heat exchange with the
203 interior ocean, and no sensible heat storage in the snow-ice system. The ice-ocean seasonal
204 energetic cycle is computed over 300 years, using climatological solar, latent and sensible heat
205 fluxes and increasing downwelling long-wave radiation, to represent the greenhouse effect. Ice
206 retreat and advance dates are diagnosed from model outputs (see Appendix A for details). We argue
207 that the Semtner (1976) zero-layer approach is appropriate to study the response of CMIP5 models
208 to warming, as the CMIP5 models with more complicated thermodynamics cannot be distinguished
209 from those using the Semtner 0-layer approach (Massonnet et al., 2018). The zero-layer approach is
210 known to alter the sea ice seasonal cycle (Semtner, 1984), but should not fundamentally affect the
211 processes discussed here.

212

213 3. Link between earlier ice retreat and later ice advance in observations and models

214 3.1 Trends in ice advance and retreat date in observations and models

215 Over 1980-2015, the ice-free season duration has increased by 9.8 ± 12.1 days/decade, with
216 nearly equal contributions of earlier ice retreat (-4.8 ± 7.7 days/decade) and later ice advance ($4.9 \pm$
217 5.8 days/decade, median based on satellite observation, updated figures, see Table S1). Variability is
218 high however. Significant trends in both d_r and d_f at the 95% confidence level are found over a
219 relatively small fraction (22%) of the seasonal ice zone (Fig. 3), independently of the details of the
220 computation (Tab. S1). The patterns of changes are regionally contrasted, and Chukchi Sea is the
221 most notable exception to the rule, where later ice advance clearly dominates changes in the ice-free
222 season (Serreze et al., 2016, Fig. 3).

223 Simulated trends by the mean of selected CMIP5 models are comparable with observations, in
224 terms of ice retreat date (-4.4 ± 3.5 days/decade), ice advance date (5.9 ± 3.3 days/decade) and ice-
225 free season duration (10.3 ± 6.3 days/decade, Fig. 3). Individual models show larger errors (Fig. S4
226 to compare with Fig.3), to be related notably with mean state issues, or to the spread in the strength
227 of strong oceanic currents, in the North Atlantic and the North Pacific. One common location where
228 trends are underestimated is the North Atlantic region, in particular Barents Sea, which arguably
229 reflects a weak meridional oceanic heat supply (Serreze et al., 2016). One should remind that as reality
230 is a single realization of internal climate variability (Notz, 2015), a model-observation comparison of
231 this kind is intrinsically limited. This could be of particular relevance in the Barents Sea, which is
232 subject to internally-generated decadal scale variations driven by ocean heat transport anomalies
233 (Yeager et al., 2015).

234

235 3.2 Earlier sea ice retreat implies later ice advance

236 In terms of mean state and contemporary trends, models seem realistic enough for an analysis
237 of changes at pan-Arctic scales but might be less meaningful at regional scales. We first study the

contemporary link between earlier retreat and ice advance by looking at the sign of $R_{a/r}$'s in contemporary observations and models. Because $R_{a/r}^{long}$ is a ratio of significant trends, and because all models have regional differences as to where trends are significant, we base our analysis on individual models.

Based on observations (Fig. 4), we find positive values of $R_{a/r}^{long}$ in more than 99% of grid points in the studied zone, provided that computations are restricted where trends on ice retreat and advance dates are significant at a 95% level (N=5257). In a warming climate, Positive $R_{a/r}^{long}$ values mean concomitant and significant trends towards earlier retreat and later advance, whereas missing values reflect either that the trends are not significant or that the point is out of the seasonal ice zone. $R_{a/r}^{short}$ (Fig. 6) is generally smaller (0.21 ± 0.27) than $R_{a/r}^{long}$ (0.71 ± 0.42 , 95% confidence level), and also positive in most pixels (87% of 23475 pixels).

CMIP5 models are consistent with the robust link between earlier ice retreat and later advance dates found in observations (Stammerjohn et al., 2012; Stroeve et al., 2016). More generally, we find a robust link between earlier retreat and later advance in all cases: both $R_{a/r}$'s are virtually always positive for short and long-term computations, from observations and models (Fig. 4, 5) over the three analysed periods (1980-2015 for observations and models, 2015-2050 and 2050-2085 for models only) and regardless of internal variability (Fig S5 and S6). This finding expands previous findings from satellite observations using detrended time series (Stammerjohn et al., 2012; Serreze et al, 2016; Stern and Laidre, 2016), in particular the clear linear correlation found between detrended ice retreat and ice advance dates (Stroeve et al., 2016). Following these authors, we attribute the strong earlier retreat / later ice advance relationship as a manifestation of the ice-albedo feedback: earlier ice retreat leads to an extra absorption of heat by the upper ocean. This heat must be released back to the atmosphere before the ice can start freezing again, leading to later ice advance. Such mechanism, also supported by satellite SST analysis in the ice-free season (Steele et al., 2008; Steele and Dickinson, 2016), explains the sign of the changes in ice advance date. However, it does not explain the relatively

263 larger magnitude of the trends in ice advance date as compared with trends in ice retreat date, studied
264 in the next section.

265 3.3 Increasingly late ice advance dominates future changes in open water season

266 We now focus on the respective contribution of changes in retreat and ice advance dates to the
267 increasingly long open water season, by analysing the magnitude of $R_{a/r}^{long}$. Contemporary values of
268 $R_{a/r}^{long}$ match between model and observations but not spatially (Fig. 4). Over 1980-2015 the simulated
269 $R_{a/r}^{long}$ (CMIP5 mean) is slightly higher (1.1 ± 0.7) than the observational value (0.7 ± 0.4). Since none
270 of the models positions the sea ice edge correctly everywhere, it is not surprising that the spatial
271 distribution and the modal $R_{a/r}^{long}$ differs among models and between models and observations. The
272 fact that, by definition, satellite data only sample one realization of internal variability could
273 contribute to the discrepancy as well. In support of these two arguments, the forced-atmosphere ISPL-
274 CM simulation better simulates the spatial distribution of $R_{a/r}^{long}$ (see Fig. S7), which underlines the
275 role of mean state errors.

276 As far as future changes are concerned, all models show a qualitatively similar evolution (Fig.
277 1 and S5). Projected changes in ice retreat and ice advance dates start by approximately 2000 and
278 continue at a nearly constant pace from 2040 until 2200. By 2040, the trend in ice advance date
279 typically becomes larger than the trend in ice retreat date, as indicated by the corresponding mean
280 $R_{a/r}^{long} = 1.8 \pm 0.4$ over 2000-2200 (Table 1).

281 To further understand these contrasting trends between ice retreat and ice advance dates, we
282 mapped $R_{a/r}^{long}$, over 2015-2050 and 2050-2085. We find that, in the course of the 21st century, trends
283 in retreat and ice advance date become significant over increasingly wide regions. The overall $R_{a/r}^{long}$
284 value increases, as illustrated in Fig. 4. This behaviour is found independent of the considered model
285 and of the internal variability (Fig. S5 and S6).

286 This finding expands the recent analyses of the CESM Large-Ensemble project (Barnhart et al.,
287 2016); and of Alaskan Arctic sea ice in CMIP5 models, finding faster ice coverage decrease in fall
288 than in spring (Wang and Overland, 2015). Both studies propose that the extra heat uptake in the
289 surface ocean due to an increased open water season as a potential explanation. As suggested earlier,

290 this indeed explains why $R_{a/r}^{long}$ would be positive but does not explain the amplified delay in ice
 291 advance date, that is, why $R_{a/r}^{long}$ would be > 1 . We are now addressing this question.

292

293 3.4 A thermodynamic mechanism for an amplified delay in ice advance date

294 The reason why $R_{a/r}^{long}$ becomes > 1 by 2040 is related to the asymmetric response of ice-ocean
 295 thermodynamics to warming: the upper ocean absorbs solar radiation about twice as efficiently as it
 296 can release heat right before ice advance. That summer feedback processes dominate is enabled by a
 297 relatively weak winter feedback (between later ice advance and earlier retreat the next year).

298 To come to this statement, we would need diagnostics unavailable in CMIP5, in particular a
 299 daily description of the surface energy budget. This is why we used a 1D thermodynamic model of
 300 sea ice growth and melt in relation with the upper ocean energy budget (Semtner, 1976), to study the
 301 idealised thermodynamic response of seasonal ice to a radiative forcing perturbation. Without any
 302 particular tuning, the 1D model simulations feature an evolution that is similar to the long-term
 303 behaviour of CMIP5 models (Fig. 1b), with trends in ice advance date (8.2 days/decade) of larger
 304 absolute magnitude than trends in retreat date (-4.7 days/decade), giving a corresponding value of
 305 $R_{a/r}^{long} = 1.9$. All figures fall within the CMIP5 envelope (Tab. 1).

306 As explained above, the seasonal relationships between ice advance and retreat dates are
 307 underpinned by atmosphere-ice-ocean feedbacks. The non-radiative feedback framework of Goosse
 308 et al. (2018, see Appendix A for details) clarifies the study of these relationships. Changes in dates
 309 of ice retreat (Δd_r) and advance (Δd_a) in response to a radiative forcing perturbation are split into
 310 reference and feedback response terms:

$$311 \quad \begin{cases} \Delta d_r = \Delta d_r^{ref} - \lambda_w \Delta d_a, \\ \Delta d_a = \Delta d_a^{ref} - \lambda_s \Delta d_r. \end{cases}$$

312 The sign convention for the feedback terms is such that the link between earlier retreat ($\Delta d_r < 0$)
 313 and later advance ($\Delta d_a > 0$) gives positive feedback factors. The feedback response refers to the

change in d_r (resp. d_a) that can solely be attributed to the change in d_a (resp. d_r). It is expressed using a feedback factor λ_w (resp. λ_s) related to winter (resp. summer) feedback processes. The reference response Δd_r^{ref} (resp. Δd_a^{ref}) is that of a virtual system in which the feedback would be absent. Expressions for the reference and feedback response terms, as well as for feedback factors stem from physical analysis, detailed in Appendix A.

According to this analysis, feedbacks between the dates of retreat and advance dominate the thermodynamic response of ice seasonality (Fig. 5): the reference response to the applied perturbation of $0.1 \text{ W/m}^2/\text{yr}$ is -0.2 d/yr of earlier retreat and 0.1 d/yr of later advance.

Ice growth and melt processes generate a relatively weak *winter* amplifying feedback of ice advance date onto ice retreat date: a shorter growth season implies thinner ice, that subsequently melts away faster. The winter feedback factor is (see Appendix A for derivation)

$$\lambda_w = \frac{1}{2} \cdot \left(\frac{d_r - d_h}{d_h - d_a} \right),$$

where d_h is the date of maximum ice thickness, is solely function of the ice growth and melt seasonal parameters. λ_w has a rather stable value of 0.31 ± 0.04 over the 127 years of simulated seasonal ice. This value of λ_w indicates a feedback response in ice retreat date of about $\sim 1/3$ of the change towards later ice advance the previous fall. λ_w is < 1 for two reasons. First the melt season is shorter than the growth season (Perovich et al., 2003), hence changes in ice advance date translate into weaker changes in ice retreat date. Second, the ice growth rate is larger for thin than for thick ice (Maykut, 1986), hence the maximum winter ice thickness does not decrease due to later advance as much as if the growth rate was constant.

Energetics of the summer ice-free ocean generate a *summer* amplifying feedback of ice retreat date onto ice advance date, much stronger than the winter feedback. The summer feedback factor is (see Appendix A for derivation)

$$\lambda_s = -\frac{\langle Q_+ \rangle}{\langle Q_- \rangle},$$

338 where $\langle Q_+ \rangle$ and $\langle Q_- \rangle$ are the average net positive (negative) atmosphere-to-ocean heat fluxes during
 339 the ice free-period. 1D model diagnostics give an average value of 1.63 ± 0.18 for λ_s , meaning that
 340 earlier retreat implies a feedback delay in ice advance of ~ 1.6 times the initial change in ice retreat
 341 date. Physically, the strength of the summer feedback is in direct relation with the ice-free upper
 342 ocean energy budget and the evolution of SST. $\langle Q_+ \rangle$ mostly corresponds to net solar flux, typically
 343 150 W/m^2 , and is typically larger than $\langle Q_- \rangle$, which corresponds to the net non-solar, mostly long-
 344 wave heat flux, at freezing temperatures, typically $75\text{-}150 \text{ W/m}^2$ (See Appendix B). Hence, after ice
 345 retreat, the SST rapidly increases due to solar absorption into the mixed layer and then decreases
 346 much slower until freezing, due to non-solar ocean-to-atmosphere fluxes (Fig. 7a), an evolution that
 347 is similar to a recent satellite-based analysis (Steele and Dickinson, 2016). In other words, the energy
 348 excess associated with later retreat, stored into the surface ocean, takes extra time to be released
 349 before ice advance.

350 In practise, keeping only the dominant term, $R_{a/r}^{long}$ (the seasonality of the system) reduces to
 351 the summer feedback factor:

$$352 \quad R_{a/r}^{long} \approx \lambda_s, \quad (4)$$

353 $R_{a/r}^{long}$ appears to vary little among CMIP5 models and even with the 1D model. Why this could be
 354 the case is because the winter and summer feedback factors are controlled by very basic physical
 355 processes of the Arctic ice-ocean-climate system, and therefore feature relatively low uncertainty
 356 levels. Celestial mechanics, ubiquitous clouds and near-freezing temperatures provide strong
 357 constraints on the surface radiation balance, hence on the summer feedback factor, that all models
 358 likely capture. All models also include the growth and melt season asymmetry and the growth-
 359 thickness relationship (see Massonnet et al., 2018) at the source of the relatively weak winter
 360 feedback. In IPSL-CM5A-LR, the sole model for which we could retrieve daily SST (Fig. 7b), the
 361 evolution of the summer SST in seasonally ice-free regions features a rapid initial increase followed
 362 by slow decrease, an indication that the mechanism we propose is sensible.

363 3.5 Inter-annual variability and extra processes add to the purely thermodynamic response

364 The CMIP5 response of ice seasonality differs from the idealised thermodynamic response in
365 two notable ways. First, $R_{a/r}^{long} > 1$ only clearly emerges by 2040 in CMIP5 models. Second, $R_{a/r}^{long}$ is
366 typically < 1 over the recent past (1980-2015) from the satellite record (Fig. 4). This must be due to
367 the contribution of processes absent from the 1D model.

368 As to why the 1D response would emerge in the course of this century, there are a series of
369 potential reasons that we cannot disentangle with the limited available CMIP5 outputs. (i) The
370 contribution of the sub-surface ocean to the surface energy budget, neglected in the 1D approach, is
371 likely larger today than in the future Arctic. Over the 21st century, the Arctic stratification increases
372 in CMIP5 models (Vancoppenolle et al., 2013; Steiner et al., 2014), whereas the oceanic heat flux
373 convergence should decrease (Bitz et al, 2005). (ii) The solar contribution to the upper ocean energy
374 budget is smaller today than in the future, as the date of retreat falls closer to the summer solstice.
375 (iii) The surface energy budget is less spatially coherent today than in the future, when the seasonal
376 ice zone moves northwards. The solar radiation maximum drastically changes over 45 to 65°N but
377 has small spatial variations above the Arctic circle (Peixoto and Oort, 1992). Note that in some
378 specific regions, $R_{a/r}^{long}$ is already > 1 , in particular in Chukchi Sea, but this has been associated to the
379 summer oceanic heat transport through Bering Strait (Serreze et al., 2016) which is a localized event,
380 that does not explain why $R_{a/r}^{long}$ would globally become > 1 in the future.

381 The aforementioned processes, ignored in the 1-D model may explain why $R_{a/r}^{long} > 1$ would
382 emerge by mid-century, but internal variability, also absent in the 1-D model, should also be
383 considered (Barnhart et al., 2016). It is remarkable that $R_{a/r}^{short}$ is < 1 both from satellite records and
384 from CMIP5 model simulations, for all periods and models considered (Fig. 6). This suggests that the
385 ice advance amplification mechanism is not dominant at inter-annual time scales. Indeed, based on
386 inter-annual satellite time series, the standard deviation of ice retreat (STD=21.6 days) and advance
387 dates (STD=14.3 days) is high (Stroeve et al., 2016) and the corresponding trends over 1980-2015

388 are not significant. Conceivably, atmosphere, ocean and ice horizontal transport, operating at synoptic
389 to inter-annual time scales, obscure the simple thermodynamic relation between the ice retreat and
390 advance dates found in the 1D model. For instance, the advection of sea ice on waters with
391 temperature higher than the freezing point would imply earlier ice advance. Altogether, this highlights
392 that the ice advance amplification mechanism is a long-term process and stress the importance of the
393 considered time scales and period as previous studies have already shown (Parkinson et al., 2014;
394 Barnhart et al., 2016).

395

396 4. Summary and discussion

397 The analysis presented in this paper, focused on changes in sea ice seasonality and the
398 associated driving mechanisms, raised the following new findings:

399 1. All CMIP5 models consistently project that the trend towards later advance progressively
400 exceeds and ultimately doubles the trend towards earlier retreat over this century, causing the ice-free
401 season to shift into fall.

402 2. The long-term shift into fall of the ice-free season is a basic feature of the thermodynamic
403 response of seasonal ice to warming.

404 3. The thermodynamic shift into fall of the ice-free season is caused by the combination of
405 relatively strong summer and relatively weak winter feedback processes.

406 4. Thermodynamic processes only explain the long-term response of ice seasonality, not the
407 inter-annual variations, nor the delayed emergence of the long-term response, which are both
408 consistently simulated features among CMIP5 models.

409 A central contribution of this paper is the detailed study of the mechanisms shaping the
410 thermodynamic response of sea ice seasonality to radiative forcing in the Semtner (1976) ice-ocean
411 thermodynamic model, using the non-radiative feedback framework of Goosse et al. (2018). The low
412 seawater albedo as compared with ice and the enhanced solar radiation uptake by the ocean had
413 previously been put forward to explain the increase in the length of the open water season
414 (Stammerjohn et al., 2012). Our analysis completes this view. Extra solar heat reaching the ocean due
415 to earlier ice retreat is absorbed at a higher rate than it can be released until ice advance. This provides
416 a powerful feedback at the source of the shift into fall of the open water season. In addition, the link
417 between later advance and earlier retreat the next spring is weak, because of the damping effects of
418 the long ice growth period and of the inverse relationship between growth rate and ice thickness. All
419 of these processes are simple enough to be captured by most of the climate models, which likely
420 explains why the different models are so consistent in terms of future ice seasonality.

421

422 The link between earlier ice retreat and later advance is found in both satellite retrievals and
423 climate projections, regardless of the considered period and time scale, expanding findings from
424 previous works (Stammerjohn et al., 2012; Serreze et al, 2016; Stern and Laidre, 2016; Stroeve et al.,
425 2016) and further stressing the important control of thermodynamic processes on sea ice seasonality.
426 Yet, two notable features are in contradiction with the thermodynamic response of seasonal ice to
427 warming. First, the long-term response of ice seasonality to warming only appears by mid-century in
428 CMIP5 simulations, when changes in the ice-free season emerge out of variability (Barnhart et al.,
429 2016). Second, changes in ice retreat date are larger than changes in ice advance date at inter-annual
430 time scales. Transport or coupling processes (involving the atmosphere, sea ice, ocean) are the most
431 likely drivers but their effect could not be formally identified because of the lack of appropriate
432 diagnostics in CMIP5. Such setup, with a long-term control by thermodynamic processes has other
433 analogues in climate change studies (Bony et al., 2004; Kröner et al., 2017; Shepherd, 2014),

434 As the Arctic sea ice seasonality is a basic trait of the Arctic Ocean, a shift of the Arctic sea
435 ice-free season would also have direct ecosystem and socio-economic impacts. The shift in the sea
436 ice seasonal cycle will progressively break the close association between the ice-free season and the
437 seasonal photoperiod in Arctic waters, a relation that is fundamental to photosynthetic marine
438 organisms existing in present climate (Arrigo and van Dijken, 2011). Indeed, because the ice advance
439 date is projected to overtake the onset of polar night (Fig. 1), typically by 2050, changes in the
440 photoperiod are at this point solely determined by the ice retreat date, and no more by advance date.
441 The duration of the sea ice season also restricts the shipping season (Smith and Stephenson, 2013;
442 Melia et al., 2017). The second clear implication of the foreseen shift of the Arctic open water season
443 is that the Arctic navigability would expand to fall, well beyond the onset of polar night, supporting
444 the lengthening of the shipping season mostly by later closing dates (Melia et al., 2017).

445

446 Better projecting future changes in sea ice and its seasonality is fundamental to our
447 understanding of the future Arctic Ocean. Detailed studies of the drivers of sea ice seasonality, in

448 particular the upper ocean energy budget, the role of winter and summer feedbacks and the respective
449 contribution of thermodynamic and dynamic processes are possible tracks towards reduced
450 uncertainties. Further knowledge can be acquired from observations (e.g. Steele and Dickinson,
451 2016) and Earth System Model analyses, for which the expanded set of ice-ocean diagnostics
452 expected in CMIP6, including daily ice concentration fields (Notz et al., 2016) will prove
453 instrumental.

454 **Code, data and sample availability**

455 Scripts available upon request.

456 Contact: Marion Lebrun, Laboratoire d'Océanographie et du Climat, IPSL Boite 100, 4 Place

457 Jussieu, 75252 Paris CEDEX 05, France.

458 Appendices

459 Appendix A: Upper ocean energetics and ice seasonality in the 1D ice-ocean model

460 To characterize the purely thermodynamic response of seasonal ice to a radiative forcing
461 perturbation, we use the Semtner (1976) zero-layer approach for ice growth and melt above an
462 upper oceanic layer taking up heat. Snow is neglected. The ice model equations for surface
463 temperature (T_{su}) and ice thickness (h) read:

$$464 \quad Q_{atm}(T_{su}) = Q_c(T_{su}), \quad (1)$$

$$465 \quad \rho L \frac{dh}{dt} = Q_{atm}(T_{su}) + Q_w. \quad (2)$$

466 where $Q_{atm} = Q_0 + Q_{sol}(1 - \alpha_i) - \epsilon \sigma T_{su}^4$, with Q_0 the sum of downwelling longwave, latent and
467 sensible heat fluxes, Q_{sol} the incoming solar flux, $\alpha_i = 0.64$ the ice albedo, $\epsilon = 0.98$ the emissivity
468 and $\sigma = 5.67 \times 10^{-8} \text{ W/m}^2/\text{K}^4$ the Stefan-Boltzmann constant. Q_c is the heat conduction flux in
469 the ice (> 0 downwards), Q_w is the ocean-to-ice sensible heat flux at the ice base, $\rho = 900 \text{ kg/m}^3$ is
470 ice density and $L = 334 \text{ kJ/kg}$ is the latent heat of fusion. Once the ice thickness vanishes, the water
471 temperature T_w in a $h_w = 30 \text{ m}$ -thick upper ocean layer follows:

$$472 \quad \rho_w c_w \frac{\partial T_w}{\partial t} h_w = Q_0 + Q_{sol}(1 - \alpha_w)[1 - \exp(-\kappa h_w)] - \epsilon \sigma T_w^4. \quad (3)$$

473 $\rho_w = 1025 \text{ kg/m}^3$ is water density, $c_w = 4000 \text{ J/kg/K}$ is water specific heat, $\kappa_w = 1/30 \text{ m}^{-1}$ is the
474 solar radiation attenuation coefficient in water. Ice starts forming back once T_w returns to the
475 freezing point $T_f = -1.8^\circ\text{C}$.

476 The atmospheric solar (Q_{sol}) and non-solar (Q_0) heat fluxes are forced using the classical standard
477 monthly mean climatologies, typical of Central Arctic conditions (Fletcher, 1965). We impose
478 $Q_w = 2 \text{ W/m}^2$ following Maykut and Untersteiner (1971). We add a radiative forcing perturbation
479 $\Delta Q = 0.1 \text{ W/m}^2$ to the non-solar flux each year to simulate the greenhouse effect. Ice becomes
480 seasonal after 127 years. The model is run until there is no ice left, which takes 324 years.

481 The following diagnostics of the ice-ocean seasonality (see Fig. A1) are derived from 1D model
482 outputs:

483 • d_r (*ice retreat date*): the first day with $T_w > T_f = -1.8^\circ\text{C}$;

484 • d_a (*ice advance date*): the last day with $T_w > T_f = -1.8^\circ\text{C}$;

485 Two other markers of the ice-ocean seasonality prove useful and were also diagnosed:

486 • d_T (*maximum water temperature date*): the last day with $Q > 0$.

487 • d_h (*maximum thickness date*): the date of maximum ice thickness.

488 The simulated trend towards later ice advance is on average 1.9 times the trend towards earlier
489 retreat, a value consistent with the CMIP5 value. An advantage of the 1D model is that the required
490 diagnostics to investigate the ice seasonality drivers are easily available.

491 Nevertheless, the response of ice seasonality is not straightforward, because there are feedbacks
492 between ice retreat and advance dates. First, later advance delays ice growth, reduces the winter
493 maximum thickness, and, in turn, implies earlier retreat. Second, earlier retreat adds extra solar heat
494 to the upper ocean, delaying ice advance. To understand the changes in ice seasonality and
495 attributing their causes, we apply the non-radiative feedback framework introduced by Goosse et al.
496 (2018).

497 **A.1 Analysis framework**

498 We split the changes in ice retreat (Δd_r) and advance (Δd_a) dates in response to a radiative forcing
499 perturbation into *reference* and *feedback* contributions (Goosse et al., 2018):

$$500 \quad \begin{cases} \Delta d_r = \Delta d_r^{ref} - \lambda_w \Delta d_a, \\ \Delta d_a = \Delta d_a^{ref} - \lambda_s \Delta d_r. \end{cases} \quad (4)$$

501 The reference response in ice retreat date to the perturbation (Δd_r^{ref}) is defined using a virtual
 502 reference system where winter feedbacks (from d_a onto d_r) would not operate. The feedback
 503 response (Δd_r^{fb}) is the total minus the reference response and is assumed proportional to the change
 504 in ice advance date (Δd_a). Equivalently it is the part of the total change in d_r that can solely be
 505 linked to changes in d_a in the previous fall. The feedback factor λ_w quantifies the strength of this
 506 link. The sign convention is such that concomitant later advance ($\Delta d_a > 0$) and earlier retreat
 507 ($\Delta d_r > 0$) give a positive feedback factor. The definitions for the feedback and reference response
 508 terms in ice advance date are similar. The only difference is that the summer feedback factor λ_s
 509 quantifies the link between earlier retreat and later advance in the same year.

510 A.2 Winter response

511 To formulate what determines the changes in ice retreat date, we focus on the ice season (Fig. A1)
 512 and use the maximum ice thickness to connect d_a to d_r . The ice thickness increases from zero on
 513 $d = d_a$ until a maximum h^{max} reached when $d = d_h$. Stefan's law of ice growth (Stefan, 1890)
 514 gives

$$515 \quad h^{max} \approx \sqrt{-\frac{2k\langle T_{su} \rangle}{\rho L} \cdot (d_h - d_a)}, \quad (5)$$

516 where $\langle T_{su} \rangle$ is the surface temperature averaged over $[d_a, d_h]$, i.e. over the ice growth period.
 517 Stefan's law is not exact but precise enough, reproducing the simulated annual values of h^{max}
 518 within $2\pm 2\%$ of the 1D model simulation over the 197 years of seasonal ice. The other advantage of
 519 Stefan's ice thickness is to be differentiable. Defining $v = k/(\rho L h^{max})$, the change in ice thickness
 520 due to the radiative forcing perturbation is, after linearisation,

$$521 \quad \Delta h^{max} = v \cdot \langle T_{su} \rangle \cdot \left[\Delta d_a - \Delta d_h + (d_a - d_h) \frac{\Delta \langle T_{su} \rangle}{\langle T_{su} \rangle} \right]. \quad (6)$$

522 Now, to connect the maximum ice thickness to the ice retreat date, we consider the melt season. The
 523 ice melts from h^{max} on $d = d_h$ until ice thickness vanishes on $d = d_r$. Hence

$$h^{max} = \langle m \rangle \cdot (d_r - d_h), \quad (7)$$

where $\langle m \rangle$ is the average melt rate, assumed to be negative.

We now combine growth and melt seasons and eliminate h^{max} . Differentiating (7), then injecting Δh^{max} from (6) and dividing by $\langle m \rangle$, we get:

$$\frac{\Delta \langle m \rangle}{\langle m \rangle} \cdot (d_r - d_h) + \Delta d_r - \Delta d_h = \frac{v \cdot \langle T_{su} \rangle}{\langle m \rangle} \cdot \left[\Delta d_a - \Delta d_h + (d_a - d_h) \frac{\Delta \langle T_{su} \rangle}{\langle T_{su} \rangle} \right]. \quad (8)$$

Using Stefan's law (equation 5) to replace h^{max} in the definition of v , the first factor on the right-hand side of (8) can be rewritten as:

$$\frac{v \cdot \langle T_{su} \rangle}{\langle m \rangle} = -\frac{1}{2} \cdot \left(\frac{d_r - d_h}{d_h - d_a} \right) \equiv -\lambda_w. \quad (9)$$

Substituting (9) into (8) and rearranging terms gives the desired decomposition between reference and feedback responses:

$$\Delta d_r = \Delta d_r^{ref} - \lambda_w \Delta d_a, \quad (10)$$

where the reference response gathers all terms independent on Δd_a :

$$\Delta d_r^{ref} = (1 - \lambda_w) \Delta d_h + (d_r - d_h) \cdot \left(\frac{\Delta \langle T_{su} \rangle}{2 \langle T_{su} \rangle} - \frac{\Delta \langle m \rangle}{\langle m \rangle} \right). \quad (11)$$

The terms on the right-hand side reflect the contributions of (i) changes in the date of maximum thickness, (ii) changes in surface temperature and (iii) changes in surface melt rate. The feedback term in (10) isolates the contribution of changes in ice advance date and λ_w now clearly appears as a feedback factor. To compute the forced and feedback terms from model output, the annual time series of $\langle T_{su} \rangle$, $\langle m \rangle$ and d_h were extracted from model outputs.

The proposed decomposition (10) is supported by analysis: the sum of calculated reference and feedback responses (black dashed line in Fig. A2a) matches the total change in ice retreat date as diagnosed from model output (yellow line in Fig. A2a).

A.3 Summer forced and feedback responses.

546 The link between ice advance date and the previous ice retreat date stems from the conservation of
 547 energy in the ice-free upper ocean. Once ice disappears on $d = d_r$, the upper ocean takes up energy
 548 (see Figure A1). The surface ocean temperature T_w increases from the freezing point until a
 549 maximum, reached on $d = d_T$. Then the upper ocean starts losing energy and T_w decreases,
 550 reaching the freezing point at the date of ice advance d_a . Over this temperature path, the energy
 551 gain from d_a to d_T must equal the energy loss from d_T to d_a :

$$552 \quad \langle Q_+ \rangle (d_T - d_r) = -\langle Q_- \rangle (d_a - d_T), \quad (12)$$

553 where $\langle Q_+ \rangle$ is the average net heat flux from the atmosphere to the upper ocean over $[d_r, d_T]$ and
 554 $\langle Q_- \rangle$ is the average net heat flux over $[d_{max}, d_a]$. Defining

$$555 \quad \lambda_s = -\frac{\langle Q_+ \rangle}{\langle Q_- \rangle}, \quad (13)$$

556 and rearranging terms in (12), we relate d_a to d_r via surface energy fluxes:

$$557 \quad d_a = -\lambda_s d_r + d_T (1 + \lambda_s). \quad (14)$$

558 By differentiating this expression, we get the sought decomposition between reference and feedback
 559 responses:

$$560 \quad \Delta d_a = \Delta d_a^{ref} - \lambda_s \Delta d_r. \quad (15)$$

561 The reference response groups all terms independent of Δd_r :

$$562 \quad \Delta d_r^{ref} = -d_r \Delta \lambda_s + \Delta d_T + \Delta (\lambda_s d_T). \quad (16)$$

563 The terms on the right-hand side reflect the contributions of (i) changes in energy fluxes, (ii) change
 564 in the date of maximum water temperature, and (iii) non linearities between both. The feedback
 565 term in (15) isolates the contribution of changes in ice retreat date and λ_s clearly now appears as a
 566 feedback factor. To compute the reference and feedback terms from the 1D model output, the
 567 annual time series of $\langle Q_+ \rangle$, $\langle Q_- \rangle$ and d_T were extracted.

568 Analysis supports the proposed decomposition: the sum of calculated feedback and reference
 569 responses (black dashed curve in Fig. A2a) is equal to the total response diagnosed from model
 570 outputs (yellow curve in Fig. A2a).

571 A.4 Analysis

572 Forced and feedback responses clarify the drivers of the shift into fall that characterises the
573 thermodynamic response of ice seasonality to the perturbation of the radiative forcing. The response
574 of the system is dominated by changes in ice advance date, which are by far dominated by the
575 feedback response (0.8 d/yr), much larger than the reference response (0.1 d/yr, see Fig. A2a). The
576 summer feedback factor λ_s , equal on average to 1.63, largely amplifies changes in retreat date. The
577 positive sign of λ_s indicates that earlier retreat implies later advance. Why $\lambda_s > 1$ is because
578 positive heat fluxes into the ocean $\langle Q_+ \rangle$ are typically larger than the heat losses $\langle Q_- \rangle$ that follow the
579 ocean temperature maximum. Hence it takes more time for the surface ocean to release the extra
580 energy than it takes to absorb it.

581 The response of ice retreat date, following winter processes, is characterised by roughly
582 equal contributions of reference (-0.2 d/yr) and feedback (-0.3 d/yr) responses. The feedback factor
583 λ_w is equal to 0.31 on average, hence changes in d_a imply changes in d_r of smaller magnitude. The
584 positive sign means that later advance implies earlier retreat. Why $\lambda_w < 1$ is because of two robust
585 features of the ice seasonal cycle that dampen the impact of changes in d_a on d_r . First the melt
586 season is shorter than the growth season, hence changes in ice advance date translate into weaker
587 changes in ice retreat date. Second, the ice growth rate is larger for thin than for thick ice, hence the
588 maximum winter ice thickness does not decrease due to later advance as much as if the growth rate
589 was constant. (The $1/h$ dependence in growth rate explains the extra 0.5 factor in λ_w).

590 Now considering the ice *advance vs. retreat amplification coefficient*, it can be expressed as
591 a function of feedback and reference responses:

$$592 \quad R \equiv -\frac{\Delta d_a}{\Delta d_r} = \lambda_s + \frac{\Delta d_a^{ref}}{\Delta d_r}. \quad (17)$$

593 R and its two contributors are depicted in Fig. A2b. Summer feedbacks largely dominate R , such
594 that $R \approx \lambda_s$ is a reasonable approximation.

595 Let us finally note that both feedback factors are determined by fundamental physical
596 features of ice-ocean interactions, likely going beyond climate uncertainties. The winter feedback is
597 determined by the shape of the seasonal cycle and the non-linear dependence of ice growth rate,
598 which are likely invariant across models. As for the summer feedback, the scaling detailed in
599 Appendix 2, indicates that the related feedback factor is constrained by celestial mechanics,
600 ubiquitous clouds and near-freezing temperatures. This likely contributes to the low level of
601 uncertainty in R among the different climate models.

602 **Appendix B: scaling of the ice-free ocean energy budget**

603 1D model results show a direct link between, on the one hand, the ratio of long-term trends in ice
604 advance and retreat date ($R_{a/r}^{long}$), and the energetics of the ice-free ocean on the other hand:

$$605 \quad R_{a/r}^{long} \approx \lambda_s = -\langle Q_+ \rangle / \langle Q_- \rangle,$$

606 where $\langle Q_+ \rangle$ and $\langle Q_- \rangle$ are the average net positive (negative) atmosphere-to-ocean heat fluxes
607 during the ice free-period. CMIP5 and 1D model results suggest that over long-time scales, this
608 ratio is stable and does not vary much among models, with values ranging from 1.5 to 2. Why this
609 ratio would be so little variable is because celestial mechanics, ubiquitous clouds and near-freezing
610 temperatures provide strong constraints on the radiation balance, which dominates the surface
611 energy budget.

612 Assuming that non-solar components cancel each other, the mean heat gain is mostly solar:

$$613 \quad \langle Q_+ \rangle = \langle Q_{sol}(1 - \alpha_w)[1 - \exp(-\kappa h_w)] \rangle_{early\ ice-free\ season},$$

614 where the mean is taken over the first part of the ice-free period, typically covering July or June. Of
615 remarkable importance is that the magnitude of clear-sky solar flux above the Arctic Circle deviates

616 by less than 20 W/m², both in space and time, around the summer solstice (see, e.g., Peixoto and
617 Oort, 1992). Assuming summer cloud skies would remain the norm, we take 150 W/m² as
618 representative for $\langle Q_+ \rangle$.

619 The mean heat loss is mostly non-solar:

620
$$\langle Q_- \rangle = \langle Q_{lw} - \epsilon \sigma T_w^4 + Q_{sh} + Q_{lh} \rangle_{late\ ice-free\ season},$$

621 and corresponds to the second part of the ice-free period, typically covering August to October.

622 Downwelling long-wave radiation flux Q_{lw} corresponds to cloud skies at near freezing
623 temperatures, for which 250 W/m² seems reasonable (Persson et al., 2002). The thermal emission
624 would be that of the ocean, a nearly ideal black body, at near-freezing temperatures, and should not
625 depart much from 300 W/m². The sensible (Q_{sh}) and latent (Q_{lh}) heat fluxes are relatively more
626 uncertain. In current ice-covered conditions, turbulent fluxes imply a net average heat loss, typically
627 smaller than 10 W/m² (Persson et al., 2002). Over an ice-free ocean however, turbulent heat losses
628 would obviously increase, in particular through the latent heat flux, but also become more variable
629 at synoptic time scales. Assuming that turbulent heat fluxes would in the future Arctic compare to
630 what they are today in ice-free ocean regions of the North Pacific, we argue that they would
631 correspond to a 25 W/m² heat loss, definitely not exceeding 100 W/m² (Yu et al., 2008).

632 Taken together, these elements give an estimated R value ranging from 1 to 2, where uncertainties
633 on the dominant radiation terms of the energy budget are small and inter-model differences in
634 turbulent heat fluxes would be decisive in determining the actual value of the ratio.

635

636 **Author Contribution**

637 All authors conceived the study and co-wrote the paper. ML and MV performed analyses.

638

639 **Competing contribution**

640 The authors declare that they have no conflict of interest.

641

642 **Acknowledgements**

643 We thank Sebastien Denvil for technical support; and Roland Seferian, Jean-Baptiste Sallée, Olivier
644 Aumont and Laurent Bopp for scientific discussions. We also thank the anonymous reviewers for
645 their constructive comments that helped to improve the paper.

646 **References**

- 647 Arrigo, K. R. and van Dijken, G. L.: Secular trends in Arctic Ocean net primary production, J.
648 Geophys. Res., 116(C9), C09011, doi:[10.1029/2011JC007151](https://doi.org/10.1029/2011JC007151), 2011.
- 649 Assmy, P., Fernández-Méndez, M., Duarte, P., Meyer, A., Randelhoff, A., Mundy, C. J., Olsen, L.
650 M., Kauko, H. M., Bailey, A., Chierici, M., Cohen, L., Doulgeris, A. P., Ehn, J. K., Fransson, A.,
651 Gerland, S., Hop, H., Hudson, S. R., Hughes, N., Itkin, P., Johnsen, G., King, J. A., Koch, B. P.,
652 Koenig, Z., Kwasniewski, S., Laney, S. R., Nicolaus, M., Pavlov, A. K., Polashenski, C. M.,
653 Provost, C., Rösel, A., Sandbu, M., Spreen, G., Smedsrud, L. H., Sundfjord, A., Taskjelle, T.,
654 Tatarek, A., Wiktor, J., Wagner, P. M., Wold, A., Steen, H. and Granskog, M. A.: Leads in Arctic
655 pack ice enable early phytoplankton blooms below snow-covered sea ice, Scientific Reports, 7,
656 srep40850, doi:[10.1038/srep40850](https://doi.org/10.1038/srep40850), 2017.
- 657 Barnhart, K. R., Miller, C. R., Overeem, I. and Kay, J. E.: Mapping the future expansion of Arctic
658 open water, Nature Clim. Change, 6(3), 280–285, doi:[10.1038/nclimate2848](https://doi.org/10.1038/nclimate2848), 2016.
- 659 Bitz, C. M., Holland, M. M., Hunke, E. C. and Moritz, R. E.: Maintenance of the Sea-Ice Edge, J.
660 Climate, 18(15), 2903–2921, doi:[10.1175/JCLI3428.1](https://doi.org/10.1175/JCLI3428.1), 2005.
- 661 Blanchard-Wrigglesworth, E., Armour, K. C., Bitz, C. M. and DeWeaver, E.: Persistence and
662 Inherent Predictability of Arctic Sea Ice in a GCM Ensemble and Observations, J. Climate, 24(1),
663 231–250, doi:[10.1175/2010JCLI3775.1](https://doi.org/10.1175/2010JCLI3775.1), 2010.
- 664 Bony, S., Dufresne, J.-L., Treut, H. L., Morcrette, J.-J. and Senior, C.: On dynamic and
665 thermodynamic components of cloud changes, Climate Dynamics, 22(2–3), 71–86,
666 doi:[10.1007/s00382-003-0369-6](https://doi.org/10.1007/s00382-003-0369-6), 2004.
- 667 Cavalieri, D. J. and Parkinson, C. L.: Arctic sea ice variability and trends, 1979–2010, The
668 Cryosphere, 6(4), 881–889, doi:[10.5194/tc-6-881-2012](https://doi.org/10.5194/tc-6-881-2012), 2012.
- 669 Collins, W. J., Bellouin, N., Doutriaux-Boucher, M., Gedney, N., Halloran, P., Hinton, T., Hughes,
670 J., Jones, C. D., Joshi, M., Liddicoat, S., Martin, G., O’Connor, F., Rae, J., Senior, C., Sitch, S.,

671 Totterdell, I., Wiltshire, A. and Woodward, S.: Development and evaluation of an Earth-System
 672 model – HadGEM2, *Geosci. Model Dev.*, 4(4), 1051–1075, doi:[10.5194/gmd-4-1051-2011](https://doi.org/10.5194/gmd-4-1051-2011), 2011.

673 Comiso, Josephino `Joey`: Bootstrap Sea Ice Concentrations from Nimbus-7 SMMR and DMSP
 674 SSM/I-SSMIS, Version 2, doi:[10.5067/J6JQLS9EJ5HU](https://doi.org/10.5067/J6JQLS9EJ5HU), 2000.

675 Dufresne, J.-L., Foujols, M.-A., Denvil, S., Caubel, A., Marti, O., Aumont, O., Balkanski, Y.,
 676 Bekki, S., Bellenger, H., Benshila, R., Bony, S., Bopp, L., Braconnot, P., Brockmann, P., Cadule,
 677 P., Cheruy, F., Codron, F., Cozic, A., Cugnet, D., Noblet, N. de, Duvel, J.-P., Ethé, C., Fairhead, L.,
 678 Fichefet, T., Flavoni, S., Friedlingstein, P., Grandpeix, J.-Y., Guez, L., Guilyardi, E., Hauglustaine,
 679 D., Hourdin, F., Idelkadi, A., Ghattas, J., Joussaume, S., Kageyama, M., Krinner, G., Labetoulle, S.,
 680 Lahellec, A., Lefebvre, M.-P., Lefevre, F., Levy, C., Li, Z. X., Lloyd, J., Lott, F., Madec, G.,
 681 Mancip, M., Marchand, M., Masson, S., Meurdesoif, Y., Mignot, J., Musat, I., Parouty, S., Polcher,
 682 J., Rio, C., Schulz, M., Swingedouw, D., Szopa, S., Talandier, C., Terray, P., Viovy, N. and
 683 Vuichard, N.: Climate change projections using the IPSL-CM5 Earth System Model: from CMIP3
 684 to CMIP5, *Clim Dyn*, 40(9–10), 2123–2165, doi:[10.1007/s00382-012-1636-1](https://doi.org/10.1007/s00382-012-1636-1), 2013.

685 Dussin, R., B. Barnier and L. Brodeau, *The making of Drakkar forcing set DFS5*. Tech. report
 686 DRAKKAR/MyOcean Report 01-04-16, LGGE, Grenoble, France. (2016).

687 Fletcher, J. O., The heat budget of the Arctic Basin and its relation to climate, Rep. R-444-PR,
 688 RAND Corp., Santa Monica, Calif., (1965).

689 Gent, P. R., Danabasoglu, G., Donner, L. J., Holland, M. M., Hunke, E. C., Jayne, S. R., Lawrence,
 690 D. M., Neale, R. B., Rasch, P. J., Vertenstein, M., Worley, P. H., Yang, Z.-L. and Zhang, M.: The
 691 Community Climate System Model Version 4, *J. Climate*, 24(19), 4973–4991,
 692 doi:[10.1175/2011JCLI4083.1](https://doi.org/10.1175/2011JCLI4083.1), 2011.

693 Giorgetta Marco A., Jungclaus Johann, Reick Christian H., Legutke Stephanie, Bader Jürgen,
 694 Böttinger Michael, Brovkin Victor, Crueger Traute, Esch Monika, Fieg Kerstin, Glushak Ksenia,
 695 Gayler Veronika, Haak Helmuth, Hollweg Heinz-Dieter, Ilyina Tatiana, Kinne Stefan, Kornblueh

696 Luis, Matei Daniela, Mauritsen Thorsten, Mikolajewicz Uwe, Mueller Wolfgang, Notz Dirk, Pithan
 697 Felix, Raddatz Thomas, Rast Sebastian, Redler Rene, Roeckner Erich, Schmidt Hauke, Schnur
 698 Reiner, Segschneider Joachim, Six Katharina D., Stockhause Martina, Timmreck Claudia, Wegner
 699 Jörg, Widmann Heinrich, Wieners Karl-H., Claussen Martin, Marotzke Jochem and Stevens Bjorn:
 700 Climate and carbon cycle changes from 1850 to 2100 in MPI-ESM simulations for the Coupled
 701 Model Intercomparison Project phase 5, *Journal of Advances in Modeling Earth Systems*, 5(3),
 702 572–597, doi:[10.1002/jame.20038](https://doi.org/10.1002/jame.20038), 2013.

703 Goosse, H., Kay, J. E., Armour, K. C., Bodas-Salcedo, A., Chepfer, H., Docquier, D., Jonko, A.,
 704 Kushner, P. J., Lecomte, O., Massonnet, F., Park, H.-S., Pithan, F., Svensson, G. and
 705 Vancoppenolle, M.: Quantifying climate feedbacks in polar regions. *Nature Communications*, 9(1),
 706 doi:[10.1038/s41467-018-04173-0](https://doi.org/10.1038/s41467-018-04173-0), 2018.

707 Hezel, P. J., Fichefet, T. and Massonnet, F.: Modeled Arctic sea ice evolution through 2300 in
 708 CMIP5 extended RCPs, *The Cryosphere*, 8(4), 1195–1204, doi:[10.5194/tc-8-1195-2014](https://doi.org/10.5194/tc-8-1195-2014), 2014.

709 Huntington, H. P., Gearheard, S., Holm, L. K., Noongwook, G., Opie, M. and Sanguya, J.: Sea ice
 710 is our beautiful garden: indigenous perspectives on sea ice in the Arctic, in *Sea Ice*, edited by D. N.
 711 Thomas, pp. 583–599, John Wiley & Sons, Ltd., 2017.

712 Johnson, M. and Eicken, H.: Estimating Arctic sea-ice freeze-up and break-up from the satellite
 713 record: A comparison of different approaches in the Chukchi and Beaufort Seas, *Elem Sci Anth*,
 714 4(0), doi:[10.12952/journal.elementa.000124](https://doi.org/10.12952/journal.elementa.000124), 2016.

715 Kröner, N., Kotlarski, S., Fischer, E., Lüthi, D., Zubler, E. and Schär, C.: Separating climate change
 716 signals into thermodynamic, lapse-rate and circulation effects: theory and application to the
 717 European summer climate, *Clim Dyn*, 48(9–10), 3425–3440, doi:[10.1007/s00382-016-3276-3](https://doi.org/10.1007/s00382-016-3276-3),
 718 2017.

719 Kwok, R. and Rothrock, D. A.: Decline in Arctic sea ice thickness from submarine and ICESat
 720 records: 1958–2008, *Geophys. Res. Lett.*, 36(15), L15501, doi:[10.1029/2009GL039035](https://doi.org/10.1029/2009GL039035), 2009.

721 Laidre, K. L., Stern, H., Kovacs, K. M., Lowry, L., Moore, S. E., Regehr, E. V., Ferguson, S. H.,
 722 Wiig, Ø., Boveng, P., Angliss, R. P., Born, E. W., Litovka, D., Quakenbush, L., Lydersen, C.,
 723 Vongraven, D. and Ugarte, F.: Arctic marine mammal population status, sea ice habitat loss, and
 724 conservation recommendations for the 21st century, *Conservation Biology*, 29(3), 724–737,
 725 doi:[10.1111/cobi.12474](https://doi.org/10.1111/cobi.12474), 2015.

726 Lindsay, R. and Schweiger, A.: Arctic sea ice thickness loss determined using subsurface, aircraft,
 727 and satellite observations, *The Cryosphere*, 9(1), 269–283, doi:[10.5194/tc-9-269-2015](https://doi.org/10.5194/tc-9-269-2015), 2015.

728 Markus, T., Stroeve, J. C. and Miller, J.: Recent changes in Arctic sea ice melt onset, freeze-up, and
 729 melt season length, *J. Geophys. Res.*, 114(C12), C12024, doi:[10.1029/2009JC005436](https://doi.org/10.1029/2009JC005436), 2009.

730 Maslanik, J., Stroeve, J., Fowler, C. and Emery, W.: Distribution and trends in Arctic sea ice age
 731 through spring 2011, *Geophys. Res. Lett.*, 38(13), L13502, doi:[10.1029/2011GL047735](https://doi.org/10.1029/2011GL047735), 2011.

732 Massonnet, F., Fichefet, T., Goosse, H., Bitz, C. M., Philippon-Berthier, G., Holland, M. M. and
 733 Barriat, P.-Y.: Constraining projections of summer Arctic sea ice, *The Cryosphere*, 6(6), 1383–
 734 1394, doi:[10.5194/tc-6-1383-2012](https://doi.org/10.5194/tc-6-1383-2012), 2012.

735 Massonnet, F., Vancoppenolle, M., Goosse, H., Docquier, D., Fichefet, T., and Blanchard-
 736 Wrigglesworth, E.: Arctic sea ice change tied to its mean state through thermodynamic processes,
 737 *Nature Climate Change*, 8(7), 599—603, 2018.

738 Maykut, G. A.: The surface heat and mass balance. In *The Geophysics of Sea Ice*, edited by N.
 739 Untersteiner, Plenum Press, New York, 146, 395-463, 1986.

740 Maykut, G. A. and Untersteiner, N.: Some results from a time-dependent thermodynamic model of
 741 sea ice, *J. Geophys. Res.*, 76(6), 1550–1575, doi:[10.1029/JC076i006p01550](https://doi.org/10.1029/JC076i006p01550), 1971.

742 Melia, N., Haines, K., Hawkins, E. and Day, J. J.: Towards seasonal Arctic shipping route
 743 predictions, *Environ. Res. Lett.*, 12(8), 084005, doi:[10.1088/1748-9326/aa7a60](https://doi.org/10.1088/1748-9326/aa7a60), 2017.

744 Notz, D.: How well climate models must agree with observations. *Philos. Trans. R. Soc. A* **373**:
745 20140164. doi:[10.1098/rsta.2014.0164](https://doi.org/10.1098/rsta.2014.0164), 2015.

746 Notz, D., Jahn, A., Holland, M., Hunke, E., Massonnet, F., Stroeve, J., Tremblay, B. and
747 Vancoppenolle, M.: The CMIP6 Sea-Ice Model Intercomparison Project (SIMIP): understanding
748 sea ice through climate-model simulations, *Geosci. Model Dev.*, 9(9), 3427–3446,
749 doi:[10.5194/gmd-9-3427-2016](https://doi.org/10.5194/gmd-9-3427-2016), 2016.

750 Notz, D. and Stroeve, J.: Observed Arctic sea-ice loss directly follows anthropogenic CO₂
751 emission, *Science*, aag2345, doi:[10.1126/science.aag2345](https://doi.org/10.1126/science.aag2345), 2016.

752 Parkinson, C. L.: Spatial patterns in the length of the sea ice season in the Southern Ocean, 1979–
753 1986, *J. Geophys. Res.*, 99(C8), 16327–16339, doi:[10.1029/94JC01146](https://doi.org/10.1029/94JC01146), 1994.

754 Parkinson, C. L.: Global Sea Ice Coverage from Satellite Data: Annual Cycle and 35-Yr Trends, *J.*
755 *Climate*, 27(24), 9377–9382, doi:[10.1175/JCLI-D-14-00605.1](https://doi.org/10.1175/JCLI-D-14-00605.1), 2014.

756 Peixoto, J. P. and Oort, A. H.: *Physics of Climate*, 1992 ed., American Institute of Physics, New
757 York., 1992.

758 Perovich, D. K., Grenfell, T. C., Richter-Menge, J. A., Light, B., Tucker, W. B. and Eicken, H.:
759 Thin and thinner: Sea ice mass balance measurements during SHEBA, *Journal of Geophysical*
760 *Research: Oceans*, 108(C3), doi:[10.1029/2001JC001079](https://doi.org/10.1029/2001JC001079), 2003.

761 Perovich, D. K., Light, B., Eicken, H., Jones, K. F., Runciman, K. and Nghiem, S. V.: Increasing
762 solar heating of the Arctic Ocean and adjacent seas, 1979–2005: Attribution and role in the ice-
763 albedo feedback, *Geophys. Res. Lett.*, 34(19), L19505, doi:[10.1029/2007GL031480](https://doi.org/10.1029/2007GL031480), 2007.

764 Persson, P. O. G., Fairall, C. W., Andreas, E. L., Guest, P. S. and Perovich, D. K.: Measurements
765 near the Atmospheric Surface Flux Group tower at SHEBA: Near-surface conditions and surface
766 energy budget, *Journal of Geophysical Research (Oceans)*, 107, 8045, doi:[10.1029/2000JC000705](https://doi.org/10.1029/2000JC000705),
767 2002.

768 Renner, A. H. H., Gerland, S., Haas, C., Spreen, G., Beckers, J. F., Hansen, E., Nicolaus, M. and
 769 Goodwin, H.: Evidence of Arctic sea ice thinning from direct observations, *Geophys. Res. Lett.*,
 770 41(14), 5029–5036, doi:[10.1002/2014GL060369](https://doi.org/10.1002/2014GL060369), 2014.

771 Rotstayn, L. D., Jeffrey, S. J., Collier, M. A., Dravitzki, S. M., Hirst, A. C., Syktus, J. I. and Wong,
 772 K. K.: Aerosol- and greenhouse gas-induced changes in summer rainfall and circulation in the
 773 Australasian region: a study using single-forcing climate simulations, *Atmos. Chem. Phys.*, 12(14),
 774 6377–6404, doi:[10.5194/acp-12-6377-2012](https://doi.org/10.5194/acp-12-6377-2012), 2012.

775 Rousset, C., Vancoppenolle, M., Madec, G., Fichefet, T., Flavoni, S., Barthélemy, A., Benshila, R.,
 776 Chanut, J., Levy, C., Masson, S. and Vivier, F.: The Louvain-La-Neuve sea ice model LIM3.6:
 777 global and regional capabilities, *Geosci. Model Dev.*, 8(10), 2991–3005, doi:[10.5194/gmd-8-2991-](https://doi.org/10.5194/gmd-8-2991-2015)
 778 [2015](https://doi.org/10.5194/gmd-8-2991-2015), 2015.

779 Schmidt, G. A., Kelley, M., Nazarenko, L., Ruedy, R., Russell, G. L., Aleinov, I., Bauer, M., Bauer,
 780 S. E., Bhat, M. K., Bleck, R., Canuto, V., Chen, Y.-H., Cheng, Y., Clune, T. L., Del Genio, A., de
 781 Fainchtein, R., Faluvegi, G., Hansen, J. E., Healy, R. J., Kiang, N. Y., Koch, D., Lacis, A. A.,
 782 LeGrande, A. N., Lerner, J., Lo, K. K., Matthews, E. E., Menon, S., Miller, R. L., Oinas, V., Oloso,
 783 A. O., Perlwitz, J. P., Puma, M. J., Putman, W. M., Rind, D., Romanou, A., Sato, M., Shindell, D.
 784 T., Sun, S., Syed, R. A., Tausnev, N., Tsigaridis, K., Unger, N., Voulgarakis, A., Yao, M.-S. and
 785 Zhang, J.: Configuration and assessment of the GISS ModelE2 contributions to the CMIP5 archive,
 786 *J. Adv. Model. Earth Syst.*, 6(1), 141–184, doi:[10.1002/2013MS000265](https://doi.org/10.1002/2013MS000265), 2014.

787 Semtner, A. J.: On modelling the seasonal thermodynamic cycle of sea ice in studies of climatic
 788 change, *Climatic Change*, 1, 27-37, 1984.

789 Semtner, A. J.: A Model for the Thermodynamic Growth of Sea Ice in Numerical Investigations of
 790 Climate, *J. Phys. Oceanogr.*, 6(3), 379–389, doi:[10.1175/1520-](https://doi.org/10.1175/1520-0485(1976)006<0379:AMFTTG>2.0.CO;2)
 791 [0485\(1976\)006<0379:AMFTTG>2.0.CO;2](https://doi.org/10.1175/1520-0485(1976)006<0379:AMFTTG>2.0.CO;2), 1976.

792 Serreze, M. C., Crawford, A. D., Stroeve, J. C., Barrett, A. P. and Woodgate, R. A.: Variability,
 793 trends, and predictability of seasonal sea ice retreat and advance in the Chukchi Sea, *J. Geophys.*
 794 *Res. Oceans*, 121(10), 7308–7325, doi:[10.1002/2016JC011977](https://doi.org/10.1002/2016JC011977), 2016.

795 Shepherd, T. G.: Atmospheric circulation as a source of uncertainty in climate change projections,
 796 *Nature Geoscience*, 7(10), 703–708, doi:[10.1038/ngeo2253](https://doi.org/10.1038/ngeo2253), 2014.

797 Smith, L. C. and Stephenson, S. R.: New Trans-Arctic shipping routes navigable by midcentury,
 798 *PNAS*, 110(13), E1191–E1195, doi:[10.1073/pnas.1214212110](https://doi.org/10.1073/pnas.1214212110), 2013.

799 Stammerjohn, S., Massom, R., Rind, D. and Martinson, D.: Regions of rapid sea ice change: An
 800 inter-hemispheric seasonal comparison, *Geophys. Res. Lett.*, 39(6), L06501,
 801 doi:[10.1029/2012GL050874](https://doi.org/10.1029/2012GL050874), 2012.

802 Steele, M., Ermold, W. and Zhang, J.: Arctic Ocean surface warming trends over the past 100 years,
 803 *Geophys. Res. Lett.*, 35(2), L02614, doi:[10.1029/2007GL031651](https://doi.org/10.1029/2007GL031651), 2008.

804 Steele, M. and Dickinson, S.: The phenology of Arctic Ocean surface warming, *J. Geophys. Res.*
 805 *Oceans*, 121(9), 6847–6861, doi:[10.1002/2016JC012089](https://doi.org/10.1002/2016JC012089), 2016.

806 Stefan, J.: Über die Theorie der Eisbildung, insbesondere über Eisbildung im Polarmeer.
 807 *Ann. Phys. 3rd. Ser.*, 42, 269–286, 1891.

808 Steiner, N. S., Christian, J. R., Six, K. D., Yamamoto, A. and Yamamoto-Kawai, M.: Future ocean
 809 acidification in the Canada Basin and surrounding Arctic Ocean from CMIP5 earth system models,
 810 *J. Geophys. Res. Oceans*, 119(1), 332–347, doi:[10.1002/2013JC009069](https://doi.org/10.1002/2013JC009069), 2014.

811 Stern, H. L. and Laidre, K. L.: Sea-ice indicators of polar bear habitat, *The Cryosphere*, 10(5),
 812 2027–2041, doi:[10.5194/tc-10-2027-2016](https://doi.org/10.5194/tc-10-2027-2016), 2016.

813 Stroeve, J. C., Kattsov, V., Barrett, A., Serreze, M., Pavlova, T., Holland, M. and Meier, W. N.:
 814 Trends in Arctic sea ice extent from CMIP5, CMIP3 and observations, *Geophys. Res. Lett.*, 39(16),
 815 L16502, doi:[10.1029/2012GL052676](https://doi.org/10.1029/2012GL052676), 2012.

816 Stroeve, J. C., Markus, T., Boisvert, L., Miller, J. and Barrett, A.: Changes in Arctic melt season
817 and implications for sea ice loss, *Geophysical Research Letters*, 41(4), 1216–1225,
818 doi:[10.1002/2013GL058951](https://doi.org/10.1002/2013GL058951), 2014.

819 Stroeve, J. C., Crawford, A. D. and Stammerjohn, S.: Using timing of ice retreat to predict timing of
820 fall freeze-up in the Arctic, *Geophys. Res. Lett.*, 43(12), 2016GL069314,
821 doi:[10.1002/2016GL069314](https://doi.org/10.1002/2016GL069314), 2016.

822 Uotila, P., Iovino, D., Vancoppenolle, M., Lensu, M. and Rousset, C.: Comparing sea ice,
823 hydrography and circulation between NEMO3.6 LIM3 and LIM2, *Geosci. Model Dev.*, 10(2),
824 1009–1031, doi:[10.5194/gmd-10-1009-2017](https://doi.org/10.5194/gmd-10-1009-2017), 2017.

825 Vancoppenolle, M., Bopp, L., Madec, G., Dunne, J., Ilyina, T., Halloran, P. R. and Steiner, N.:
826 Future Arctic Ocean primary productivity from CMIP5 simulations: Uncertain outcome, but
827 consistent mechanisms, *Global Biogeochem. Cycles*, 27(3), 605–619, doi:[10.1002/gbc.20055](https://doi.org/10.1002/gbc.20055), 2013.

828 Voldoire, A., Sanchez-Gomez, E., Méliá, D. S. y, Decharme, B., Cassou, C., Sénési, S., Valcke, S.,
829 Beau, I., Alias, A., Chevallier, M., Déqué, M., Deshayes, J., Douville, H., Fernandez, E., Madec,
830 G., Maisonnave, E., Moine, M.-P., Planton, S., Saint-Martin, D., Szopa, S., Tyteca, S., Alkama, R.,
831 Belamari, S., Braun, A., Coquart, L. and Chauvin, F.: The CNRM-CM5.1 global climate model:
832 description and basic evaluation, *Clim Dyn*, 40(9–10), 2091–2121, doi:[10.1007/s00382-011-1259-](https://doi.org/10.1007/s00382-011-1259-y)
833 [y](https://doi.org/10.1007/s00382-011-1259-y), 2013.

834 Wang, M. and Overland, J. E.: Projected future duration of the sea-ice-free season in the Alaskan
835 Arctic, *Progress in Oceanography*, 136, 50–59, doi:[10.1016/j.pocean.2015.01.001](https://doi.org/10.1016/j.pocean.2015.01.001), 2015.

836 Wassmann, P. and Reigstad, M.: Future Arctic Ocean Seasonal Ice Zones and Implications for
837 Pelagic-Benthic Coupling, *Oceanography*, 24(3), 220–231, doi:[10.5670/oceanog.2011.74](https://doi.org/10.5670/oceanog.2011.74), 2011.

838 Wu, T., Song, L., Li, W., Wang, Z., Zhang, H., Xin, X., Zhang, Y., Zhang, L., Li, J., Wu, F., Liu,
839 Y., Zhang, F., Shi, X., Chu, M., Zhang, J., Fang, Y., Wang, F., Lu, Y., Liu, X., Wei, M., Liu, Q.,
840 Zhou, W., Dong, M., Zhao, Q., Ji, J., Li, L. and Zhou, M.: An overview of BCC climate system

841 model development and application for climate change studies, *Acta Meteorol Sin*, 28(1), 34–56,
842 doi:[10.1007/s13351-014-3041-7](https://doi.org/10.1007/s13351-014-3041-7), 2014.

843 Yeager, S. G., A. R. Karspeck, and G. Danabasoglu (2015), Predicted slowdown in the rate of
844 Atlantic sea ice loss, *Geophys. Res. Lett.*, 42, doi:[10.1002/2015GL065364](https://doi.org/10.1002/2015GL065364).

845 Yu, L., X. Jin, and R. A. Weller, Multidecade Global Flux Datasets from the Objectively Analyzed
846 Air-sea Fluxes (OAFlux) Project: Latent and sensible heat fluxes, ocean evaporation, and related
847 surface meteorological variables. Tech. Report Woods Hole Oceanographic Institution, OAFlux
848 Project Technical Report. OA-2008-01, 64pp. Woods Hole. Massachusetts (2008).

849

Tables and Figures

Table 1. Linear trends in ice retreat and advance dates over 2000-2200 (200 years), and long-term ice advance amplification ratios for the individual and mean CMIP5 models and for the 1D model. Trends and ratios are given as median \pm interquartile range over the seasonal ice zone where trends are significant at a 95% confidence level ($p = 0.05$).

	r_r (days / decade)	r_a (days / decade)	$R_{a/r}^{long}$	Reference
CCSM4	-6.6 ± 2.1	13.4 ± 7.3	2.0 ± 0.6	<i>Gent et al.</i> , 2011
CNRM-CM5	-8.0 ± 2.8	13.5 ± 5.9	1.7 ± 0.3	<i>Voldoire et al.</i> , 2013
CSIRO-Mk3-6-0	-6.1 ± 3.3	10.4 ± 4.0	1.7 ± 0.6	<i>Rotstayn et al.</i> , 2012
GISS-E2-H	-2.8 ± 0.6	5.1 ± 1.6	1.8 ± 0.4	<i>Schmidt et al.</i> , 2014
MPI-ESM-LR	-8.6 ± 2.8	15.2 ± 8.1	1.8 ± 0.4	<i>Giorgetta et al.</i> , 2013
bcc-csm1-1	-5.2 ± 1.3	9.7 ± 2.6	1.9 ± 0.4	<i>Wu et al.</i> , 2014
GISS-E2-R	-2.0 ± 0.4	3.4 ± 0.8	1.8 ± 0.3	<i>Schmidt et al.</i> , 2014
HadGEM2-ES	-9.1 ± 3.0	18.6 ± 7.6	1.9 ± 0.5	<i>Collins et al.</i> , 2011
IPSL-CM5A-LR	-5.7 ± 1.2	11.1 ± 3.8	1.9 ± 0.5	<i>Dufresne et al.</i> , 2013
MEAN CMIP5	-6.0 ± 2.0	11.1 ± 4.6	1.8 ± 0.4	
1D model	$-4.7 \pm \text{n.a.}$	$8.2 \pm \text{n.a.}$	$1.9 \pm \text{n.a.}$	

Figure 1. Evolution of the ice seasonality diagnostics (ice retreat date, blue; and ice advance date, orange): (a) CMIP5 median and interquartile range, with corresponding range of satellite derived-values (green rectangles 1980-2015) over the 70-80°N latitude band; (b) one-dimensional ice-ocean model results. The ice-free period (L_w), the photoperiod (L_p) and the average polar night (gray rectangle) are also depicted. Note that the systematic difference between observations and CMIP5 models is reduced when accounting for the systematic bias due to the daily interpolation of monthly means in CMIP5 models (See Methods and Tab. S2).

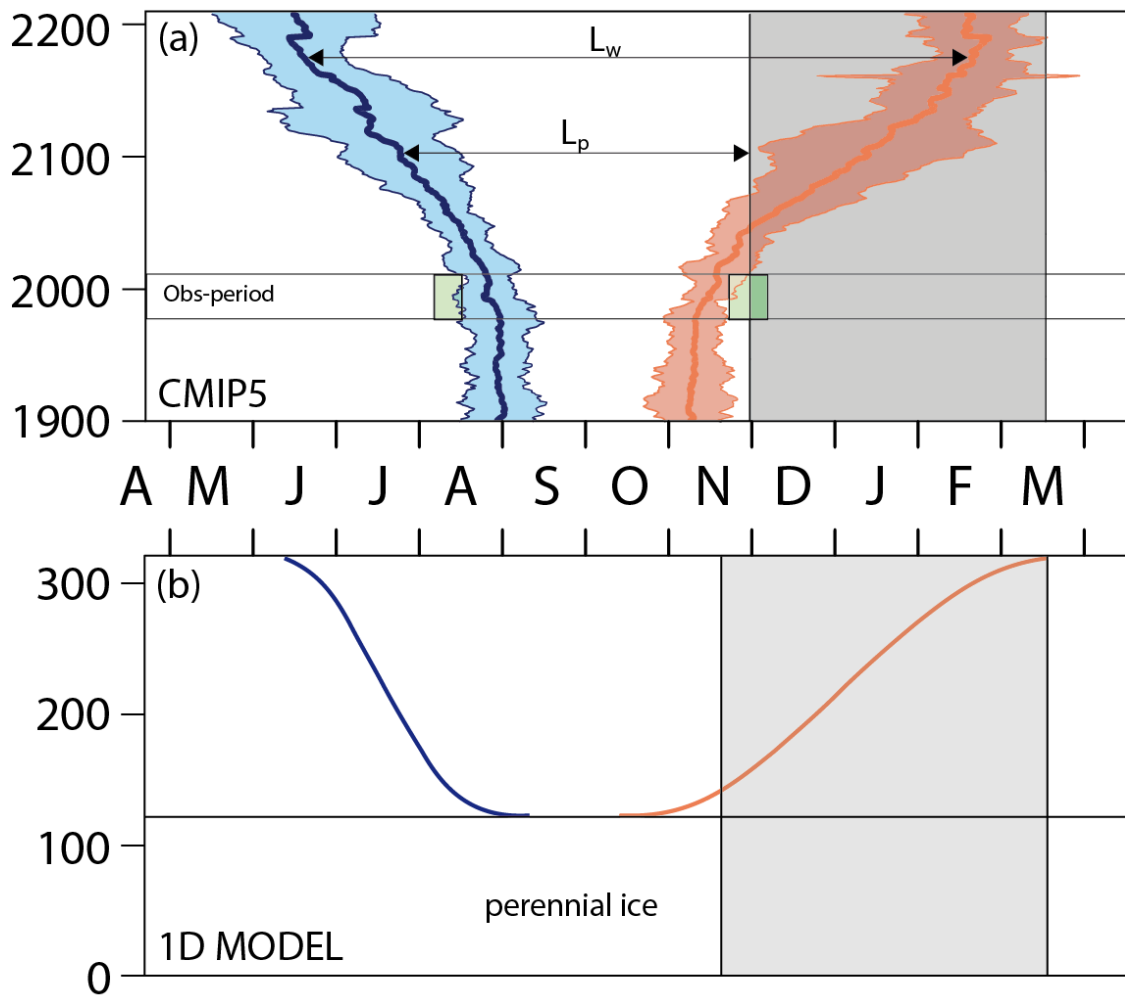


Figure 2. Maps and frequency histograms of (a,d) ice retreat date (b,e) ice advance date and (c,f) ice-free season length over 1980-2015 (36 years), based on (a,b,c) passive microwave satellite concentration retrievals (Comiso, 2000; updated 2015) and (d,e,f) daily concentration fields averaged over CMIP5 models. Median \pm IQR refers to all points in the seasonal ice zone. See figure S3 for individual models.

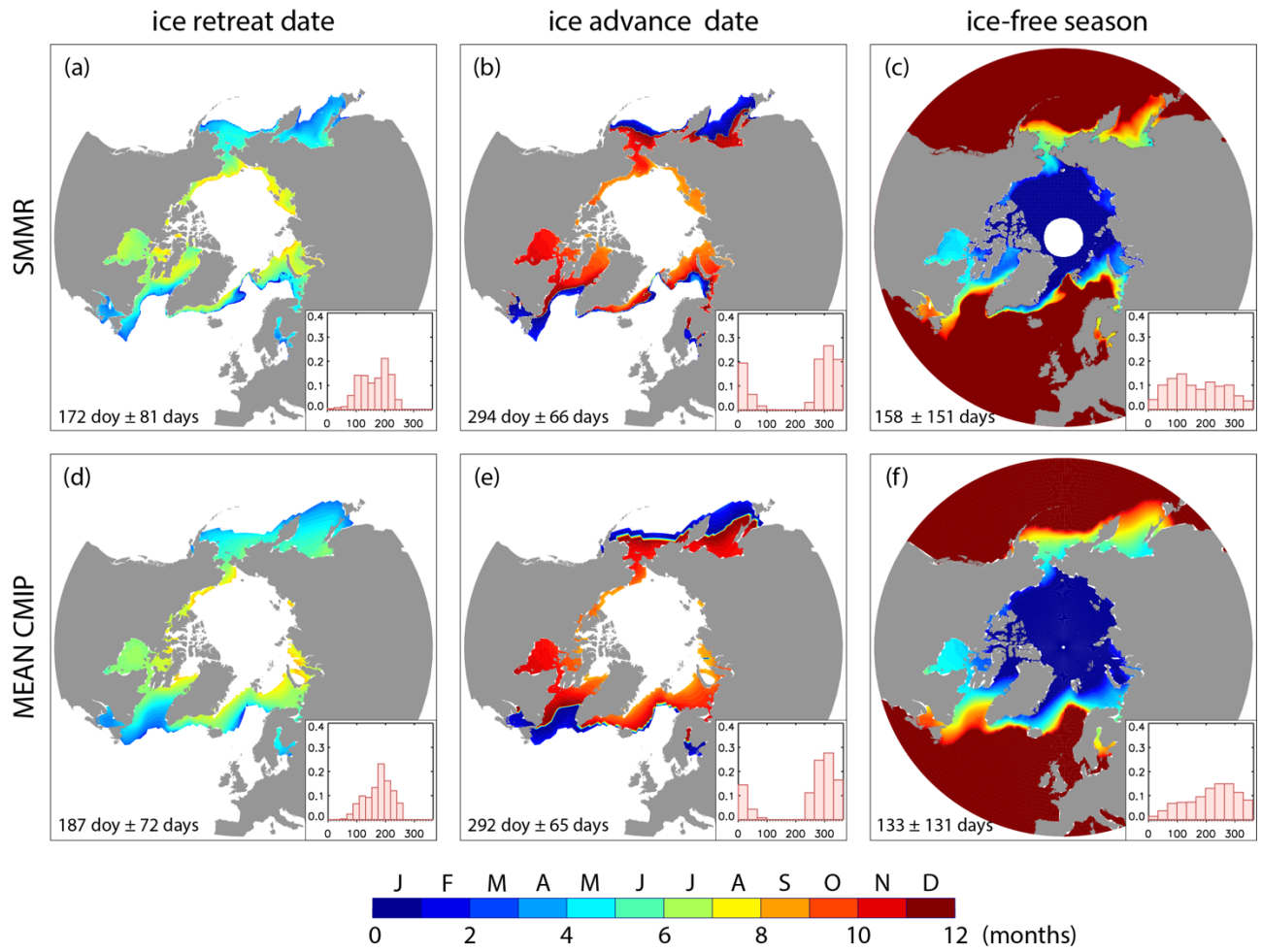


Figure 3. Maps and frequency histograms of linear trends (for hatched zones only) in (a,d) ice retreat date (b,e,) ice advance date and (c,f) ice-free season length over 1980-2015 (36 years), based on (a,b,c) passive microwave satellite concentration retrievals (Comiso, 2000; updated 2015); (d,e,f) the mean CMIP5 models. Hatching refers to the 95% confidence interval ($p=0.05$). Median \pm IQR refers to significant pixels with at least 1/3 of the years with defined retreat and ice advance dates. See figure S4 for individual models.

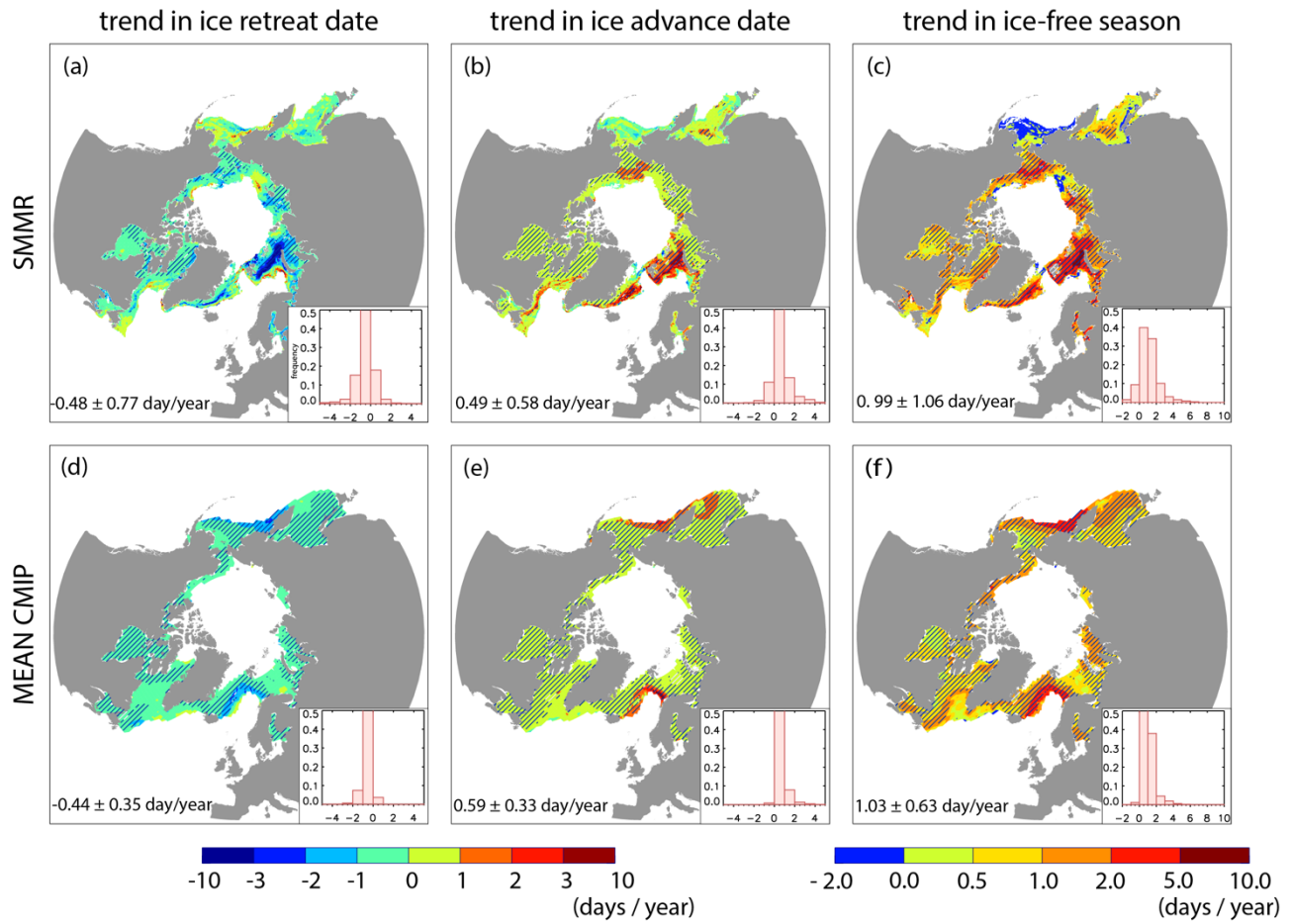


Figure 4. Long-term ice advance vs. retreat amplification coefficient from passive microwave ice concentration retrievals (SMMR; over 1980-2015); and for all individual models over 1980-2015, 2015-2050 and 2050-2085. We use a 75% ($p=0.25$) confidence interval for this specific computation. Similar figures (for SMMR and IPSL_CM5A_LR only) for $p = 0.05$ are available as Supplementary Material (Fig. S9).

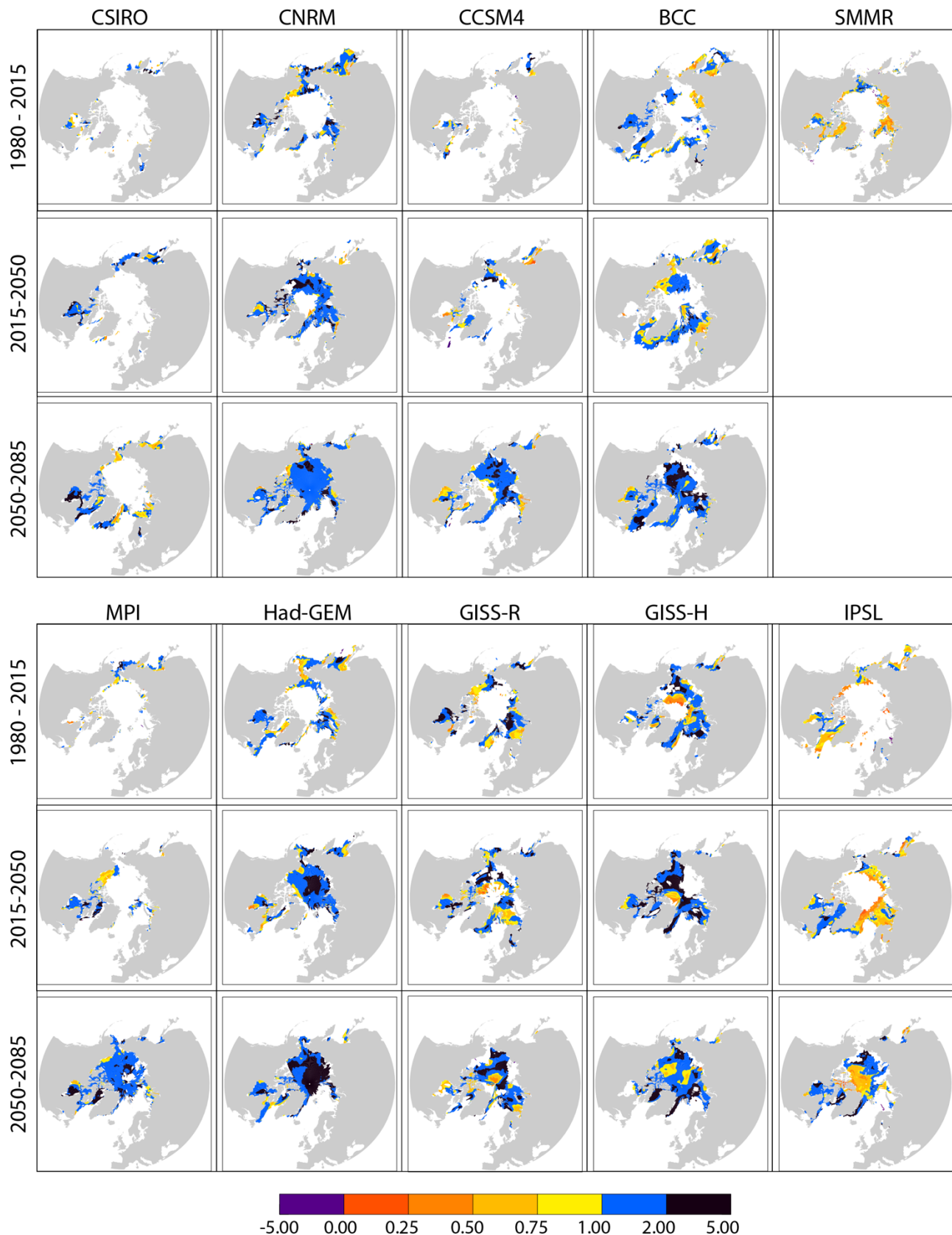


Figure 5. Schematics of the mechanisms shaping the thermodynamic response of sea ice seasonality to a radiative forcing perturbation. The numbers give annual averages simulated by the 1D model. Changes in ice retreat and advance dates are split between *reference* (*ref*) and *feedback* (*fb*) responses. See Appendix A for details of the computations.

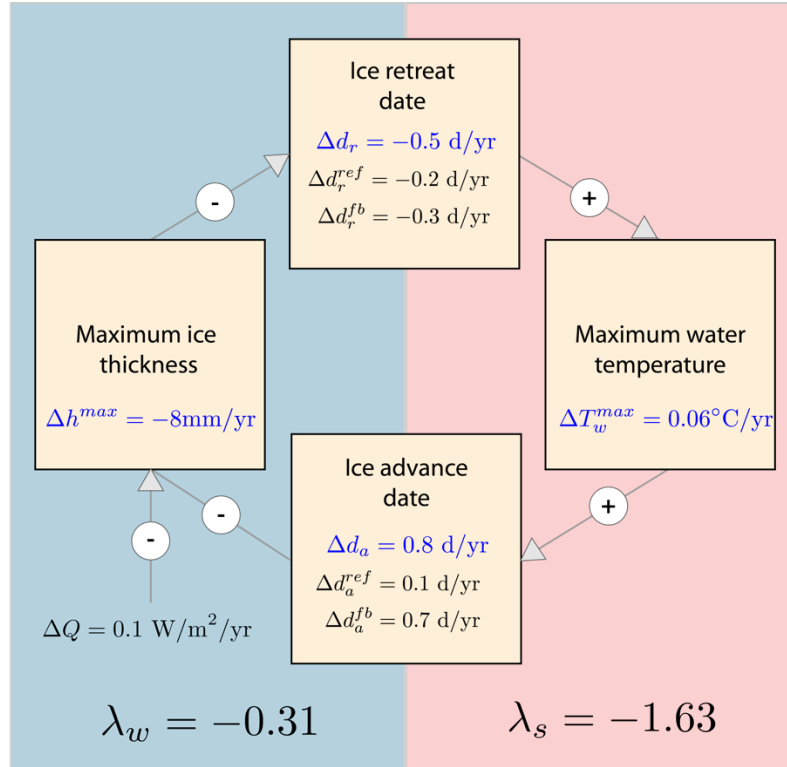


Figure 6. Short-term ice advance vs. retreat amplification coefficient from passive microwave ice concentration retrievals (SMMR; over 1980-2015); and for all individual models over 1980-2015, 2015-2050, 2050-2085.

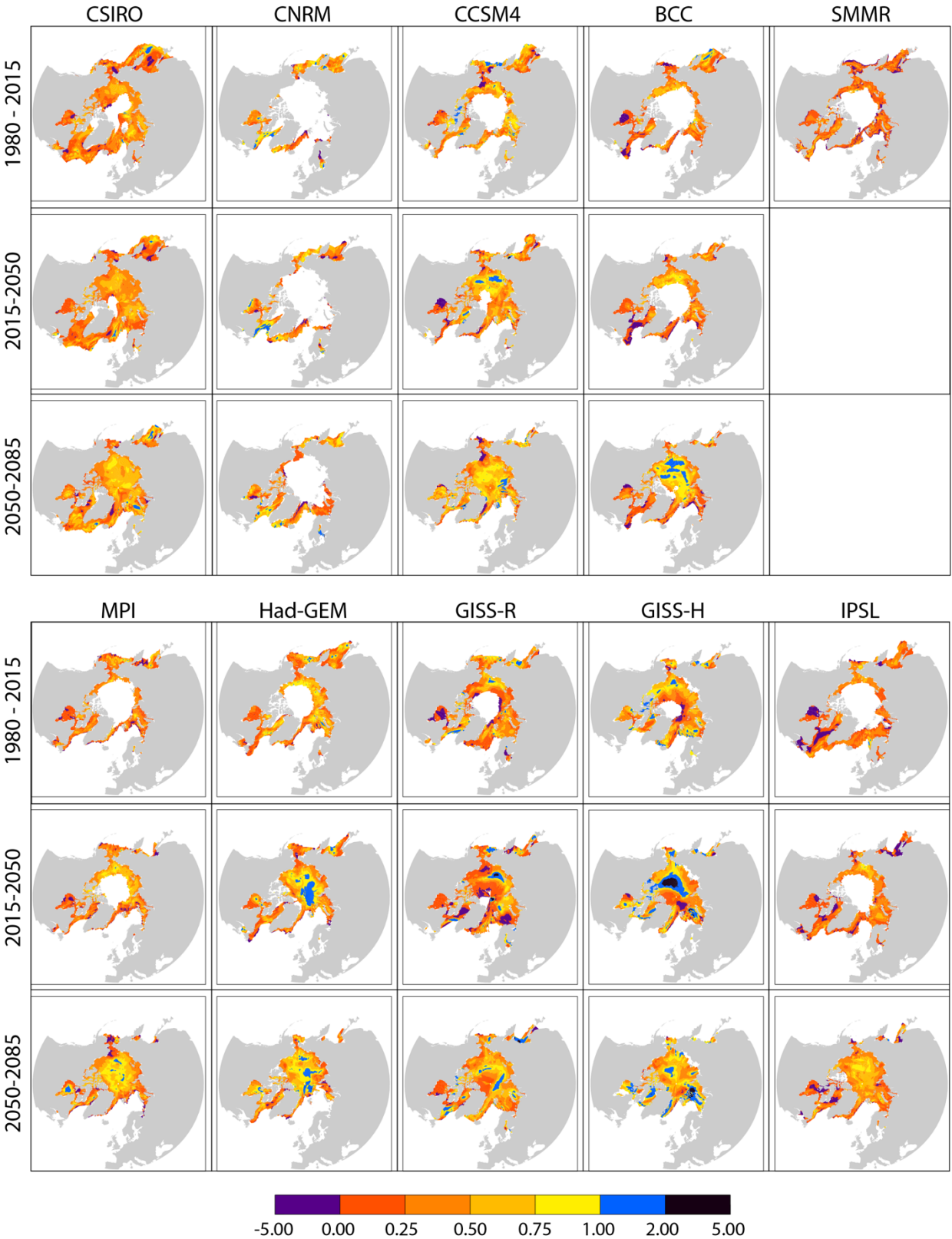


Figure 7. (Top) Energetics of ice retreat and advance in the simple model: net atmospheric (solid) and solar (yellow) heat fluxes to the ocean; SST (dash), depicted for years 150 and 210. **(Bottom)** Annual evolution of the simulated sea surface temperature, averaged over the seasonal ice zone, for two decades of reference (2015-2025, 2075-2085) as simulated by the IPSL_CM5A_LR model and showing the same temporal asymmetry as in the simple model.

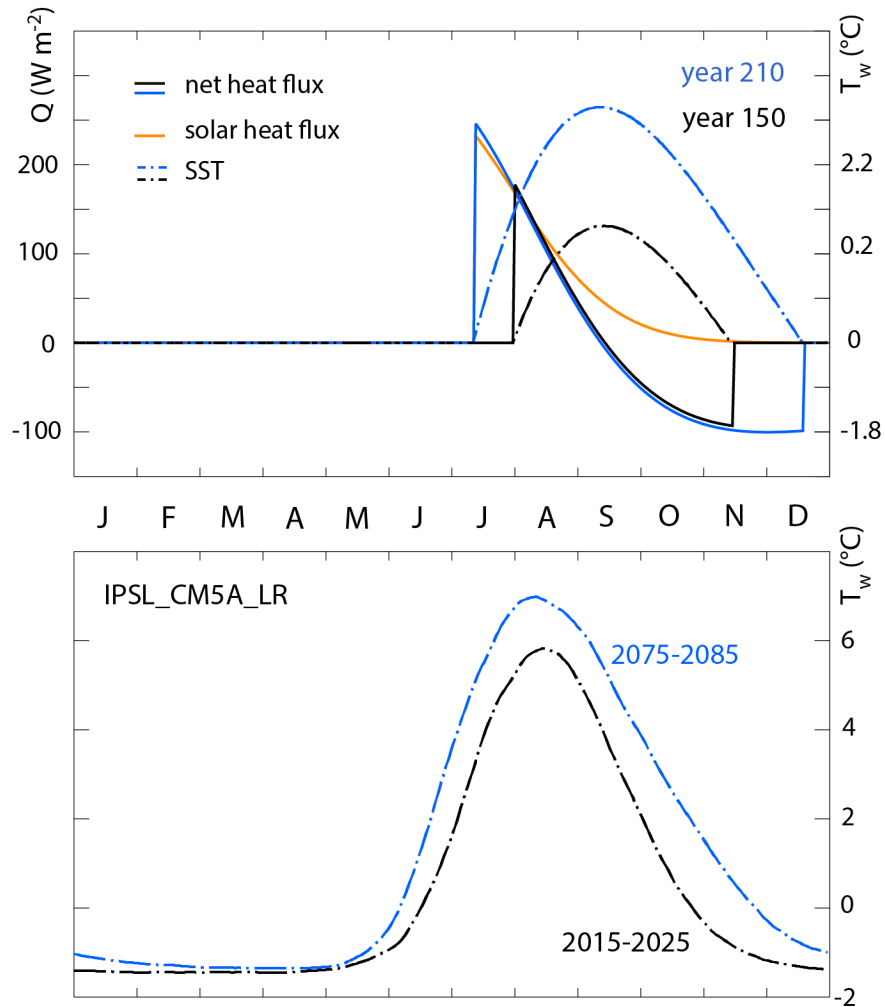


Figure A1. Schematic representation of the analysis framework applied to the 1D model outputs, illustrating the mechanisms of change in ice seasonality between a reference year (solid line/upper colors) and a subsequent year (dashed line/lower colors). Ice appears at the ice advance date (d_a). The ice thickness (h) increases until the date of maximum thickness (d_h) then decreases at an average melt rate $\langle m \rangle$. Once the ice thickness vanishes at the ice retreat date d_r , the sea water temperature T_w increases due to incoming heat flux $\langle Q_+ \rangle$, until the date of maximum temperature (d_T) and finally decreases due to the heat loss $\langle Q_- \rangle$.

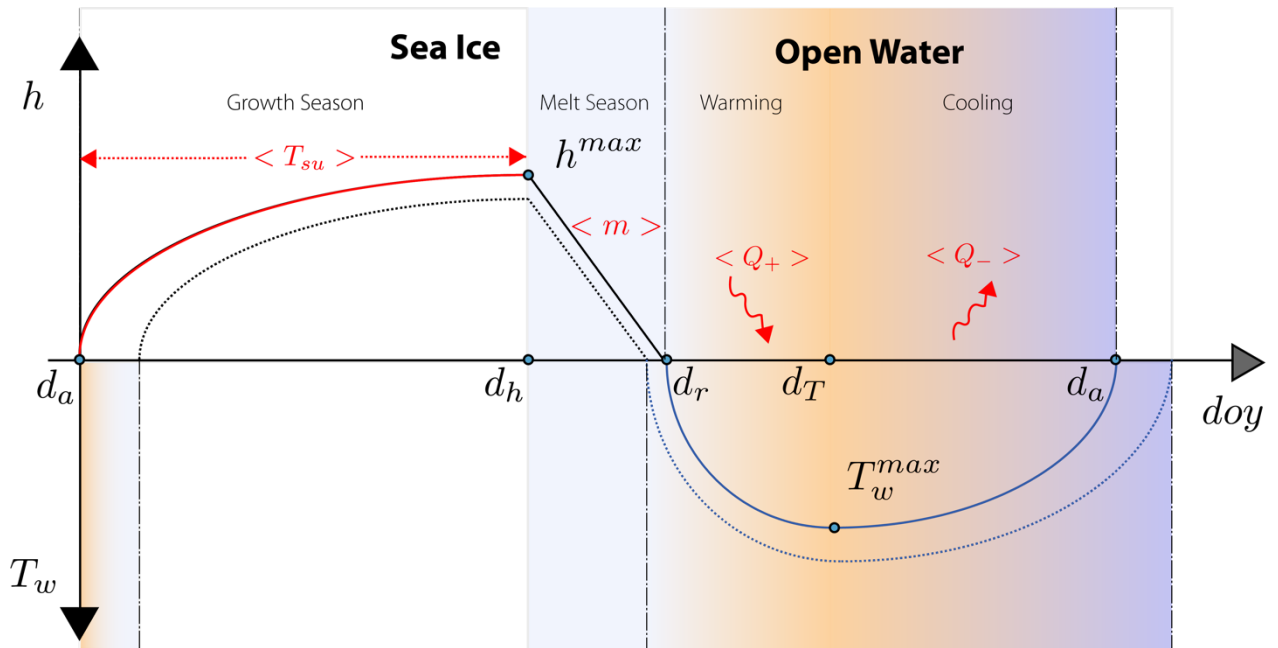


Figure A2. Thermodynamic response of sea ice seasonality to warming in the 1D model: (a) Evolution over the years of the annual contributors to changes in ice retreat and advance date, as simulated by the 1D model. The yellow line gives the total response Δd_r (resp. Δd_a) as diagnosed from model output. The blue curve gives the reference response Δd_r^{ref} (resp. Δd_a^{ref}) to the radiative forcing perturbation as calculated with eq. 11 (resp. 16). The red curve gives the feedback response Δd_r^{fb} (resp. Δd_a^{fb}), attributed to the feedback from d_a (resp. d_r), calculated with eq. 9 and 10 (resp. 13 and 15). The black dashed line testifies that the sum of reference and feedback responses matches the total. **(b) Evolution over the years of the simulated freeze-up amplification ratio in the 1D model.** The yellow curve gives the freeze-up amplification R , calculated as the ratio of the total response in d_a (Δd_a) divided by the total response in d_r (Δd_r), as diagnosed from the 1D model. The blue curve gives the contribution of the reference response to the freeze-up amplification ratio ($\Delta d_a^{ref}/\Delta d_r$). The red curve gives the contribution of the summer feedbacks ($\Delta d_a^{ref}/\Delta d_r = \lambda_s$). The black dashed line testifies that the sum of reference and feedback contributions matches the total.

